This is to certify that the
thesis entitled

FLUORESCENCE LINESHAPE STUDIES OF THERMAL UNFOLDING AND SECONDARY STRUCTURE TRANSITIONS IN PROTEINS

presented by

Sara E. McFadden

has been accepted towards fulfillment
of the requirements for the

M.S. degree in Chemistry

Warren F. Beck

Major Professor's Signature

24 May 2006

Date

MSU is an Affirmative Action/Equal Opportunity Institution

FLUORESCENCE LINESHAPE STUDIES OF THERMAL UNFOLDING AND SECONDARY STRUCTURE TRANSITIONS IN PROTEINS

By

Sara E. McFadden

A THESIS

Submitted to
Michigan State University
in partial fulfillment of the requirements
for the degree of

MASTER OF SCIENCE

Department of Chemistry

2006

ABSTRACT

FLUORESCENCE LINESHAPE STUDIES OF THERMAL UNFOLDING AND SECONDARY STRUCTURAL TRANSITIONS IN PROTEINS

By

Sara E. McFadden

Using 1-anilino-8-naphthalenesulfonic acid (ANSA) as an extrinsic hydrophobic fluorescent probe, we have monitored protein and solvent motions in the thermal unfolding and secondary structural transitions in proteins. ANSA is sensitive to the polarity of its environment. By first characterizing the lineshape of the ANSA fluorescence spectrum with respect to changes in solvent polarity, we were able to relate the changes of the lineshape to the relative change in polarity of the ANSA-binding site in the proteins under study. Analysis of all the parameters associated with the lineshape of the spectrum provided more structural information than monitoring the intensity of the fluorescence alone.

In this thesis, we examine the thermal unfolding of the molten globule of bovine α-lactalbumin and the α-helix to β-sheet secondary structure transition of poly-L-lysine. The results presented here show that the thermal unfolding of the molten globule of α-lactalbumin is not a two-state transition as was previously suggested. Using the ANSA fluorescence spectrum lineshape and Rayleigh light scattering from poly-L-lysine, we show that the transition from the α-helix form to the β-sheet form is preceded by the formation of a molten-globule-like intermediate, which then rapidly aggregates.

TO
Kate, Michele and my family

ACKNOWLEDGMENTS

I would like to thank my advisor, Dr. Warren Beck, and the Beck group for their help and support during my time at MSU. I also want to thank my family and friends for all their support.

TABLE OF CONTENTS

LIST OF TABLES

LIST OF FIGURES

LIST OF ABBREVIATIONS

ANSA	1-anilino -8-naphthalenesulfonic acid
BLA	Bovine α-lactalbumin
CD	Circular Dichroism
FTIR	Fourier Transform Infrared Spectroscopy
HCl	Hydrochloric Acid
LED	Light-Emitting Diode
MG	Molten Globule
NaOH	Sodium Hydroxide
NMR	Nuclear Magnetic Resonance
PLL	Poly-L-lysine

CHAPTER 1

INTRODUCTION

There are four basic levels of protein structure. The sequence of amino acids in the protein is known as the primary structure and the physical arrangement of the primary structure into a-helices or b-strands is known as the secondary structure. These small regions of secondary structure fold and interact with one another to form the native tertiary structure. In large proteins, domains of tertiary structure interact with one another to form the quaternary structure.[1]

One important process that has yet to be understood is that by which a sequence of amino acids folds into a specific three–dimensional protein structure.[2,3] An understanding of this process would theoretically allow a researcher with a need for a specific three–dimensional structure to determine the sequence of amino acids that would fold into the target structure. A better knowledge of how a protein folds may also give insight into what causes a protein to fold improperly or to lose its folded–state stability.

Protein misfolding is thought to be a direct cause for the transmissible spongiform encephalopathy diseases that include Cruetzfeldt-Jakob disease in humans, scrapie in sheep, and bovine spongiform encephalopathy ("mad cow disease").[4,5] Alzheimer's disease and Parkinson's disease are amyloidoses which are also associated with protein misfolding.[6,7] These diseases are thought to be associated with the accumulation of amyloid fibrils, but the critical step seems to be the decay of the native folded form of the protein in question.[2]

Native proteins have both hydrophilic topologies and hydrophobic cores. This combination allows the protein to be soluble and to protect its hydrophobic core from the solvent environment. The protection of the hydrophobic core from the solvent plays a critical role in the stability of the native fold.[8] Amyloid fibrils, which are derived from native proteins, are insoluble.[9] Proteins that fail to assume the proper native fold form small soluble aggregates that associate into protofibrils. The protofibrils go on to form insoluble mature fibrils. The initial aggregation, however, is always associated with a misfolded or partially unfolded state of the protein.[5,10]

The ability of polypeptides to form amyloid fibrils is apparently a general property and not necessarily dependent on specific amino–acid sequences or native–fold topologies.[11] The molten globule state of α–lactalbumin at low pH, and other members of the lysozyme family of proteins, have been shown to form amyloid fibrils at high salt concentrations.[12] Regardless of the protein of origin, the fully formed fibrils exhibit nearly identical structures.[5,10] The rates at which the misfolded proteins aggregate, however, depend strongly on the physicochemical properties of the proteins, such as the spatial organization of charges, a preference for certain secondary structural features, and hydrophobicity.[13]

The current trend in the debate over what role misfolded or aggregated protein structures play in the progress of disease points to small aggregate structures from misfolded proteins as the disease–causing species. It was found that structurally disorganized pre-fibrilar aggregates are highly cytotoxic while structurally well-defined mature fibrilar forms of the same protein are mostly harmless.[14-17] The pre–fibrilar forms

are thought to be toxic because they expose hydrophobic regions of the protein to the surrounding solvent.[15]

In the so–called *new view* of protein folding, there are thought to be many possible folding trajectories between the unfolded and native states on the folding potential–energy surface, which has been termed an *energy landscape*.[18-19] A funnel–shaped topology of the potential–energy surface by which folding proteins are steered toward their native states has been suggested.[20-22] This view requires consideration of the dynamics of an ensemble of folding trajectories rather than the standard two–state reaction–coordinate that is suggested by most biochemical and spectroscopic experiments.[3,23,24] It is possible that protein misfolding results from alternate Gibbs free–energy minima on the landscape that act as kinetic sinks. The picture of a protein folding funnel with local Gibbs free–energy minima suggest that the native structure is formed under a combination of kinetic and thermodynamic control.[25] Because folded proteins are only marginally stable, misfolded proteins may also form spontaneously from the native state.[20] Given that the topology of the funnel would suggest steeply sloping sides close to the native state, it is likely that most unfolding trajectories lead to refolding of the native structure.

Assuming the process by which a protein folds is similar to the process by which it unfolds, the study of protein unfolding should give information about the potential–energy surface of its folding funnel. For example, intermediates in the unfolding of a protein would suggest that there are local energy minima on the walls of the funnel. If the intermediates that collect in these kinetic traps could be isolated and

characterized, one can imagine that specific pharmaceuticals might be designed to recognize intermediates and retard the formation of the disease–causing products.

The formation of the hydrophobic core is thought to provide most of the energetic stabilization of the native fold.[7] Redfield and coworkers have shown that in α–lactalbumin, the native–like three-dimensional fold is formed through interactions of regions that are at opposite ends in the sequence code.[26] They attribute the stability of the fold to the grouping of hydrophilic and hydrophobic residues.

In this thesis, we examine the nature of events in the unfolding of the hydrophobic core in two protein systems. We use an extrinsic chromophore, 1–anilino–8–naphthalenesulfonic acid (ANSA), that is sensitive to changes in polarity to sense protein and solvent motions in partially unfolded protein states and in changes of secondary structure. First, we monitor the flow of solvent molecules into the hydrophobic core of the α-lactalbumin molten globule as it unfolds. We then monitor the formation of a molten–globule–like intermediate as poly-L-lysine undergoes a conformational change from α–helix to β–sheet.

Because of the sensitivity of ANSA (see Figure 1.1) to polarity, it has been widely used as an extrinsic probe in the study of proteins and membrane composition and function.[27-29] The fluorescence quantum yield of ANSA in water is less than 10^{-2}. As the polarity of the solvent surrounding the ANSA molecule decreases, the quantum yield increases.[28] A decrease in the quantum yield of the ANSA fluorescence with increasing solvent polarity can be attributed to a larger probability of non-radiative transitions as the larger dipole of the excited state interacts more readily with a more polar solvent.[30] A low fluorescence quantum yield of ANSA in water allows for any signal of unbound dye to be

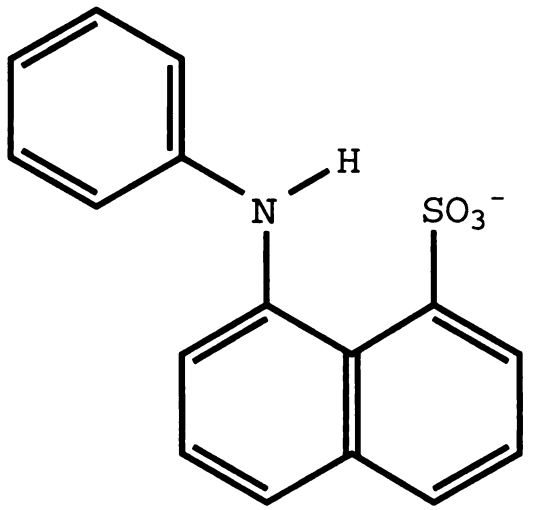

Figure 1.1. Structure of 1,8-anilinonaphthalenesulfonic acid.

neglected. Therefore, if the probe molecule is bound to a protein, any change in the ANSA spectrum can be attributed to a motion of the protein which affects the polarity of the ANSA environment. A decrease in polarity of the solvent also causes the emission maximum to shift to the blue.

The spectral changes with respect to polarity are due to solvatochromism. When the ground–state (S_0 state) probe molecule absorbs a photon, it is promoted to the first excited singlet state (S_1). In this excited state, the dipole moment of the molecule is larger than it is in the ground state. Solvent molecules that surround the excited state probe molecule rotate to align their dipole moments with the dipole moment of the excited species and lower the energy of the excited state. The more polar the solvent, the more the energy of the excited state is decreased. [31] (See Figures 1.2 and 1.3) This results in a shift of the spectrum to the red as the polarity of the solvent increases.

In this thesis, we show that a fit of the ANSA fluorescence spectrum to a log-normal lineshape[32] can provide structural information that is not provided by an analysis of intensity alone. The fit to a log-normal lineshape gives three spectral parameters: area, center frequency, and half-width at half-maximum. The area of the log-normal lineshape is proportional to the fluorescence quantum yield of the probe, the center frequency is sensitive to the polarity of the probe environment, and the half–width at half–maximum is sensitive to the range of structures and binding sites in the ensemble. A comparison of the rates at which these parameters change can provide considerably more insight into the change in probe environment with motions of the protein.

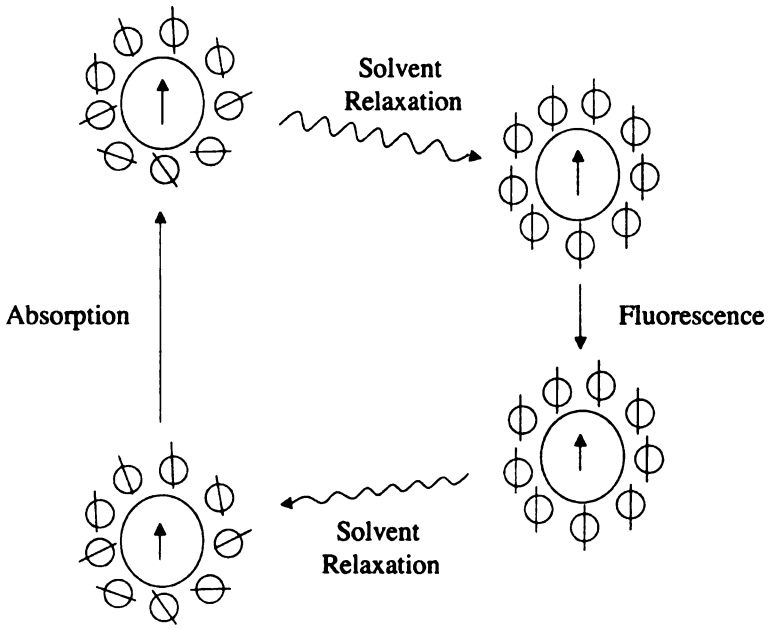

Figure 1.2. Cartoon representation of the interaction of the dipole moment of the chromophore and the surrounding solvent molecules. The large circle with an arrow represents the chromophore and its dipole moment and the small circles represent the solvent molecules and their dipole moments. After Lakowicz.[31]

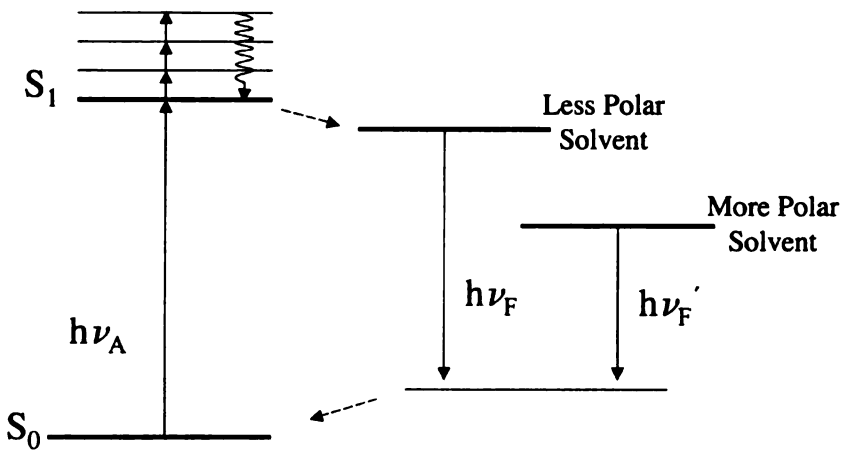

Figure 1.3. Energy level diagram corresponding to a solvatochromic probe in solvents with different polarities. S_0 is the ground state of the chromophore, S_1 is the first excited state of the chromophore, $h\nu_A$ is the energy of the absorption photon, $h\nu_F$ and $h\nu_F'$ is the energy of the fluorescence photon in a less and more polar solvent, respectively. After Lakowicz.[31]

References

(1) Branden, C.; Tooze, J. *Introduction to Protein Structure*; 2nd ed.; Garland Publishing, Inc.: New York, 1999.

(2) Dobson, C. M. "Protein folding and misfolding." *Nature* **2003**, *426*, 884–890.

(3) Dill, K. A.; Chan, H. S. "From Levinthal to pathways to funnels." *Nature Struct. Biol.* **1997**, *4*, 10–19.

(4) Dobson, C. M. "Protein misfolding, evolution and disease." *Trends Biochem.Sci.* **1999**, *24*, 329–332.

(5) Prusiner, S. B. "Prions." *Proc. Natl. Acad. Sci. USA* **1998**, *95*, 13363–13383.

(6) Caughey, B.; Lansbury, P. T. "Protofibrils, pores, fibrils, and neurodegeneration: Separating the responsible protein aggregates from the innocent bystanders." *Annu. Rev. Neurosci.* **2003**, *26*, 267–298.

(7) Selkoe, D. J. "Folding proteins in fatal ways." *Nature* **2003**, *426*, 900–904.

(8) Kauzmann, W. "Some factors in the interpretation of protein denaturation." *Adv. Protein. Chem.* **1959**, *14*, 1–63.

(9) Dobson, C. M. "The structural basis of protein folding and its links with human disease." *Philos. Trans. R. Soc. Lond. Ser. B-Biol. Sci.* **2001**, *356*, 133–145.

(10) Sunde, M.; Blake, C. "The structure of amyloid fibrils by electron microscopy and X-ray diffraction." In *Adv. Prot. Chem.*, 1997; Vol. 50, p 123–159.

(11) Chiti, F.; Webster, P.; Taddei, N.; Clark, A.; Stefani, M.; Ramponi, G.; Dobson, C. M. "Designing conditions for in vitro formation of amyloid protofilaments and fibrils." *Proc. Natl. Acad. Sci. USA* **1999**, *96*, 3590–3594.

(12) Goers, J.; Permyakov, E. A.; Permyakov, S. E.; Uversky, V. N.; Fink, A. L. "Conformational Prerequisites for α–Lactalbumin Fibrillation." *Biochemistry* **2002**, *41*, 12546.

(13) Chiti, F.; Stefani, M.; Taddei, N.; Ramponi, G.; Dobson, C. M. "Rationalization of the effects of mutations on peptide and protein aggregation rates." *Nature* **2003**, *424*, 805-808.

(14) Hartley, D. M.; Walsh, D. M.; Ye, C. P. P.; Diehl, T.; Vasquez, S.; Vassilev, P. M.; Teplow, D. B.; Selkoe, D. J. "Protofibrillar intermediates of amyloid beta-protein induce acute electrophysiological changes and progressive neurotoxicity in cortical neurons." *J. Neurosci.* **1999**, *19*, 8876–8884.

(15) Bucciantini, M.; Giannoni, E.; Chiti, F.; Baroni, F.; Formigli, L.; Zurdo, J. S.; Taddei, N.; Ramponi, G.; Dobson, C. M.; Stefani, M. "Inherent toxicity of aggregates implies a common mechanism for protein misfolding diseases." *Nature* **2002**, *416*, 507–511.

(16) Bucciantini, M.; Calloni, G.; Chiti, F.; Formigli, L.; Nosi, D.; Dobson, C. M.; Stefani, M. "Prefibrillar amyloid protein aggregates share common features of cytotoxicity." *J. Biol. Chem.* **2004**, *279*, 31374–31382.

(17) Cleary, J. P.; Walsh, D. M.; Hofmeister, J. J.; Shankar, G. M.; Kuskowski, M. A.; Selkoe, D. J.; Ashe, K. H. "Natural oligomers of the amyloid-protein specifically disrupt cognitive function." *Nat. Neurosci.* **2005**, *8*, 79–84.

(18) Frauenfelder, H.; Sligar, S. G.; Wolynes, P. G. "The energy landscapes and motions of proteins." *Science* **1991**, *254*, 1598–1603.

(19) Brooks III, C. L.; Onuchic, J. N.; Wales, D. J. "Statistical Thermodynamics: Taking a Walk on a Landscape." *Science* **2001**, *293*, 612-613.

(20) Onuchic, J. N.; Luthey-Schulten, Z.; Wolynes, P. G. "Theory of Protein Folding: The Energy Landscape Perspective." *Annu. Rev. Phys. Chem.* **1997**, *48*, 545–600.

(21) Bryngelson, J. D.; Wolynes, P. G. "Spin glasses and the statistical mechanics of protein folding." *Proc. Natl. Acad. Sci. U. S. A.* **1987**, *84*, 7524–7528.

(22) Leopold, P. E.; Montal, M.; Onuchic, J. N. "Protein folding funnels: a kinetic approach to the sequence–structure relationship." *Proc. Natl. Acad. Sci. U. S. A.* **1992**, *89*, 8721-8725.

(23) Chan, H. S.; Dill, K. A. "Protein folding in the landscape perspective: Chevron plots and Non-Arrhenius kinetics." *Proteins: Struct. Funct. Genet.* **1998**, *30*, 2–33.

(24) Dill, K. A. "Polymer principles and protein folding." *Protein Sci.* **1999**, *8*, 1166–1180.

(25) Baker, D.; Agard, D. A. "Kinetics Versus Thermodynamics in Protein-Folding." *Biochemistry* **1994**, *33*, 7505–7509.

(26) Redfield, C.; Schulman, B. A.; Milhollen, M. A.; Kim, P.; Dobson, C. M. "α–Lactalbumin forms a compact molten globule in the absence of disulfide bonds." *Nat. Struct. Biol.* **1999**, *6*, 948–952.

(27) Slavik, J. "Anilinonaphthalene Sulfonate as a Probe of Membrane Composition and Function." *Biochimica Et Biophysica Acta* **1982**, *694*, 1-25.

(28) Turner, D. C.; Brand, L. "Quantitative Estimation of Protein Binding Site Polariy. Fluorescence of *N*–Arylaminonaphthalenesulfonates." *Biochemistry* **1968**, *7*, 3381-3390.

(29) Weber, G.; Daniel, E. "Cooperative Effects in Binding by Bovine Serum Albumin. II. The Binding of 1–Anilino–8–napthalenesulfonate. Polarization of the Ligand Fluorescence and Quenching of the Protein Fluorescence." *Biochemistry* **1966**, *5*, 1900–1907.

(30) Edelman, G. M.; McClure, W. O. "Fluorescent Probes and the Conformation of Proteins." *Accounts of Chemical Research* **1968**, *1*, 65-70.

(31) Lakowicz, J. R. *Principles of Fluorescence Spectroscopy*; Second ed.; Kluwer Academic/Plenum Publishers: New York, 1999.

(32) Siano, D. B.; Metzler, D. E. "Band shapes of the electronic spectra of complex molecules." *Journal of Chemical Physics* **1969**, *51*, 1856–1861.

CHAPTER 2

LINESHAPE CHARACTERIZATION OF THE FLUORESCENCE SPECTRUM OF 1-ANILINO-8-NAPHTHALENESULFONIC ACID DURING THE THERMAL UNFOLDING OF THE α-LACTALBUMIN MOLTEN GLOBULE

Introduction

In this chapter, we characterize the change in lineshape of the 1-anilino-8-naphthalenesulfonic acid (ANSA) fluorescence spectrum during the thermal unfolding of the α-lactalbumin molten globule. As a first step, we characterize the sensitivity of the fluorescence spectrum lineshape to a change in polarity by varying the concentrations of methanol and water. Once the changes in spectral lineshape that occur in response to the change in methanol concentration have been established, we will use it as a gauge to detect changes in the hydrophobic core of the molten globule of α-lactalbumin as it unfolds.

Bovine α-lactalbumin (BLA) is a relatively small protein (~14 kDa) that plays a vital role in the production of milk in mammals.[1] It has been widely studied, however, because of its ability to readily form a stable molten globule (MG).[2] The MG state is a partially denatured state that is characterized by a native-like secondary structural component but with few native tertiary interactions and a fluctuating hydrophobic core.[3] BLA has two main domains; one domain that is primarily α -helical and a second domain that contains predominantly a β-sheet structure (see Figure 2.1).[4] Dobson and co-workers have used NMR techniques coupled with hydrogen exchange studies to show that the MG states of α-lactalbumins are structurally similar to the native states, but have expanded hydrophobic cores and lack the tight side-chain packing of the native states.[5-8] Fluorescence studies of α-lactalbumin using tryptophan residues also indicate that the

Figure 2.1. Structure of bovine α-lactalbumin with the Ca^{2+} ion rendered as a sphere. This picture created from protein data bank entry 1F6S using PyMOL.

MG state has native-like tertiary interactions but a more globular form than the native state.[9] Native BLA has been known to partially unfold to the molten globular state under the following conditions: acidic pH, high temperature, low concentration of chemical denaturants, and removal of the Ca^{2+} ion.[10] Recently, NMR data has been used to determine a "coarse-grained" free energy landscape for the folding of the MG form of human α-lactalbumin.[11]

ANSA has been shown to preferentially bind to the MG state of proteins rather than to the native or fully unfolded states. Even in proteins with hydrophobic side chains on the surface, ANSA will not readily bind to the native or fully unfolded states.[12,13] The expanded hydrophobic core of the MG allows the ANSA to bind within the core of the protein.

Using ANSA as an extrinsic probe, we can monitor the flow of solvent molecules into the hydrophobic core of MG α-lactalbumin as it unfolds. In this chapter we show that the transition from the MG state to the fully unfolded state is not a two-state transition as was previously believed from the results of Dobson and coworkers and Arai and Kuwajima.[14,15]

Sample Preparation

ANSA (8-anilino-1-naphthalenesulfonic acid ammonium salt) and BLA (α-lactalbumin from bovine milk) were obtained from Sigma and used as received. Samples were dissolved in methanol (Spectrum, spectrophotometric grade) or water as stated to obtain an absorbance of less than 0.15 at 350 nm with a 1-cm path length. The aqueous BLA samples were brought to pH 2.0 with addition of HCl. Prior to collection

of fluorescence spectra, the samples were passed through 0.22 μm filters. A 1:2 chromophore:protein molar ratio was used to limit the possibilities of a protein having more than one bound chromophore.[16]

Experimental Setup

Figure 2.2 shows a schematic diagram of the fluorescence spectrometer used in experiments discussed in this chapter. An 380-nm light-emitting diode (Ocean Optics, LS-450) was used as the excitation source. Light from the LED was directed through an 1-m optical fiber. It was then focused into the sample cuvette by a 1-inch focal length fused-silica lens.

A Quantum Northwest TLC 50 Fluorescence Cuvette Holder was used as the sample holder. The use of this sample holder allowed for heating, cooling, and stirring of the sample. The TLC 50 fluorescence cuvette holder employs a Peltier device for temperature control and requires a flow of water to cool the Peltier chip's heat sink. To prevent condensation buildup during temperature changes, the sample compartment was purged with nitrogen.

Within the sample cuvette, the focus of the 380-nm light from the excitation source was directed slightly toward the collection optics to minimize self-absorption of the fluorescence signal by the sample. A 1-inch focal length fused-silica lens was placed directly after the optical window at 90° with respect to the excitation source to collect the fluorescence emitted from the sample. A 4-inch focal length fused-silica lens focused the fluorescence signal into a Spex 270M Spectrograph. The entrance slit of the

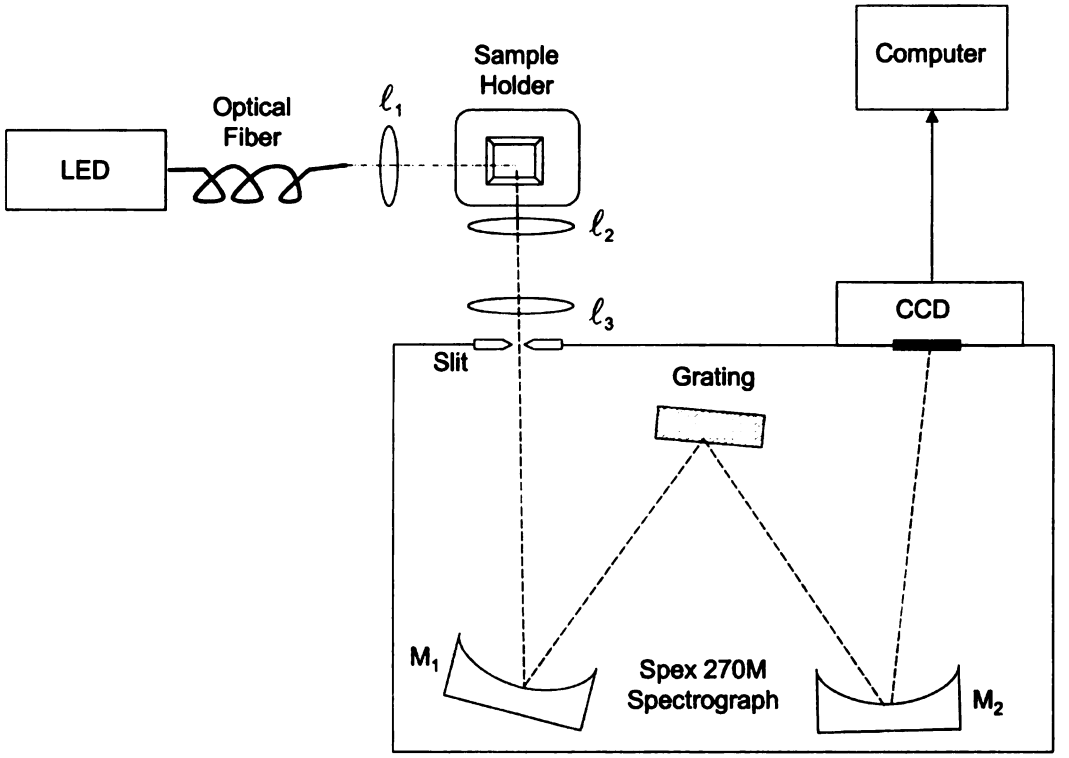

Figure 2.2. Schematic diagram of the fluorescence spectrometer used in experiments discussed in this chapter. *Symbols*: LED, 380 nm light-emitting diode light source; ℓ_1, 1-inch focal length lens; ℓ_2, 1-inch focal length lens; ℓ_3, 4-inch focal length lens; M_1, collimating mirror; M_2, focusing mirror; Grating, 600 gr/mm grating; CCD, 2048 x 512 pixel CCD detector. The temperature-controlled sample holder was a Quantum Northwest TLC 50 Fluorescence Cuvette Holder.

spectrograph was fixed at 0.5 mm giving the spectrograph an effective band pass of 3.09 nm. After passing through the entrance slit of the spectrograph, the fluorescence signal was directed at a 600-groove/mm diffraction grating by a large collimating mirror. Following the grating, a focusing mirror focused the diffracted spectrum onto a Spex SpectrumOne 2048 x 512 pixel CCD detector. The CCD was positioned at the slit plane of the spectrograph so that the emission was focused onto the CCD detector elements. A shutter on the entrance slit of the spectrograph controlled the amount of time the CCD was exposed during each experiment.

Spex SpectraMax software, as provided with the CCD detector, was used for data collection. Automation of data collection was possible using QuicKeys software to control the sequence of events in the SpectraMax software. The baseline signal from the CCD detector was removed from the fluorescence spectra through subtraction of blank solvent-only spectra that were recorded under the same measurement conditions with the same cuvette. When plotted as a function of wavenumber, the fluorescence intensity was multiplied by the square of the wavelength as required to compensate for the fixed effective spectral band pass of the spectrometer.[17]

Absorption spectra were obtained with a 2-nm spectral band pass at room temperature with a Hitachi U-2000 spectrometer and LabVIEW (National Instruments) routines.

Results

Figure 2.3 shows the fluorescence (F/ν^3) and absorption (A/ν) relative dipole-strength spectra of 5 μM ANSA in pH 2.0 water. The dipole strength measures the square of the

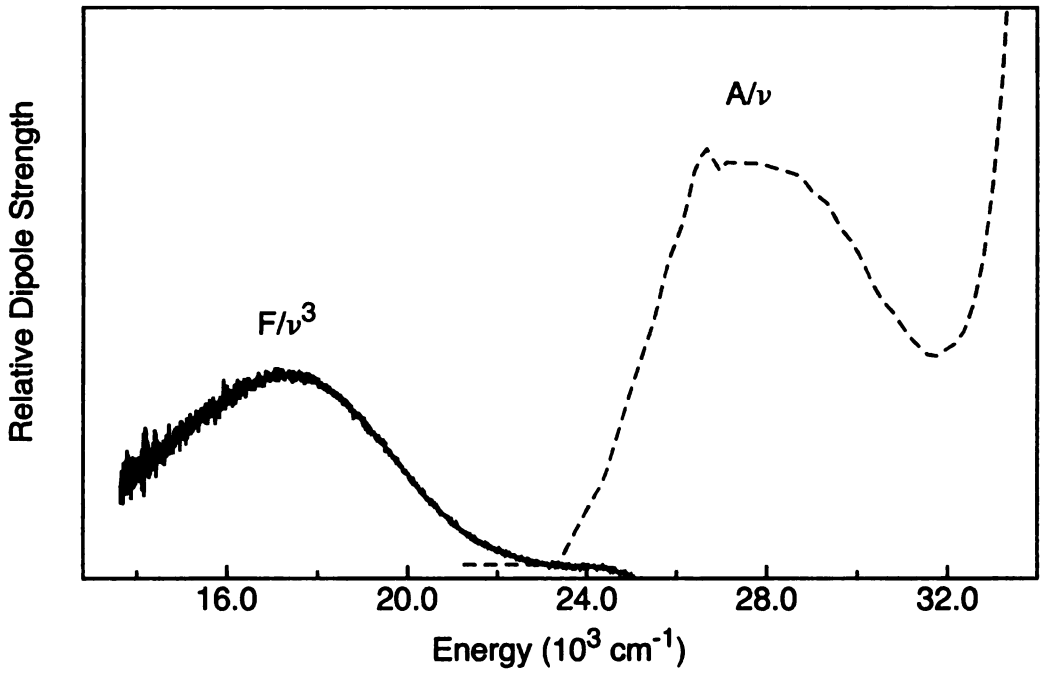

Figure 2.3. Fluorescence (F/ν^3) and absorption (A/ν) dipole-strength spectra from a solution of 5 μM ANSA in pH 2.0 water. The fluorescence spectrum is centered at 16940 cm^{-1} and the absorption spectrum is centered at 28620 cm^{-1}.

transition-dipole moment.[18] The fluorescence and absorption spectra have log-normal lineshapes[19] that are mirrored to one another with respect to the direction of the skew, or asymmetry, of the lineshape. The fluorescence spectrum is centered around 16940 cm^{-1}. The absorption spectrum is centered around 28620 cm^{-1}. The optical density of the 20 μM ANSA solution in neat methanol was 0.12. The ANSA absorption spectrum arises from a series of overlapping bands, with the one at 28620 cm^{-1} associated with the lowest singlet state from which the fluorescence arises.

The fluorescence dipole-strength spectra from solutions of 20 μM ANSA with decreasing methanol to water ratios are shown in Figure 2.4. The fluorescence spectra shown in Figure 2.4 were collected with 15-second integration times and 15 averaged accumulations. As the methanol to water ratio decreases, the polarity of the solution increases. With the increase in solvent polarity, the ANSA fluorescence spectrum decreases in relative dipole strength and shifts to the red.

Figures 2.5 – 2.7 report the change in lineshape of the ANSA fluorescence spectrum with the change in polarity of solvent. The fluorescence spectrum obtained at a given methanol concentration was fit to a log-normal lineshape. The skew, or asymmetry, of the fitted log-normal lineshape was held constant at 1.14; this parameter does not change measurably as the methanol concentration is changed. Figure 2.5 shows that as the percentage of methanol increases, the area increases exponentially. The plot of ln(dipole strength) versus percent methanol is linear. The area is equivalent to the integrated relative dipole strength, which is proportional to the fluorescence quantum yield.[18] The area of the ANSA fluorescence spectrum in 100 percent methanol is more than 75 times larger than that of the ANSA fluorescence spectrum in 99.5 percent water.

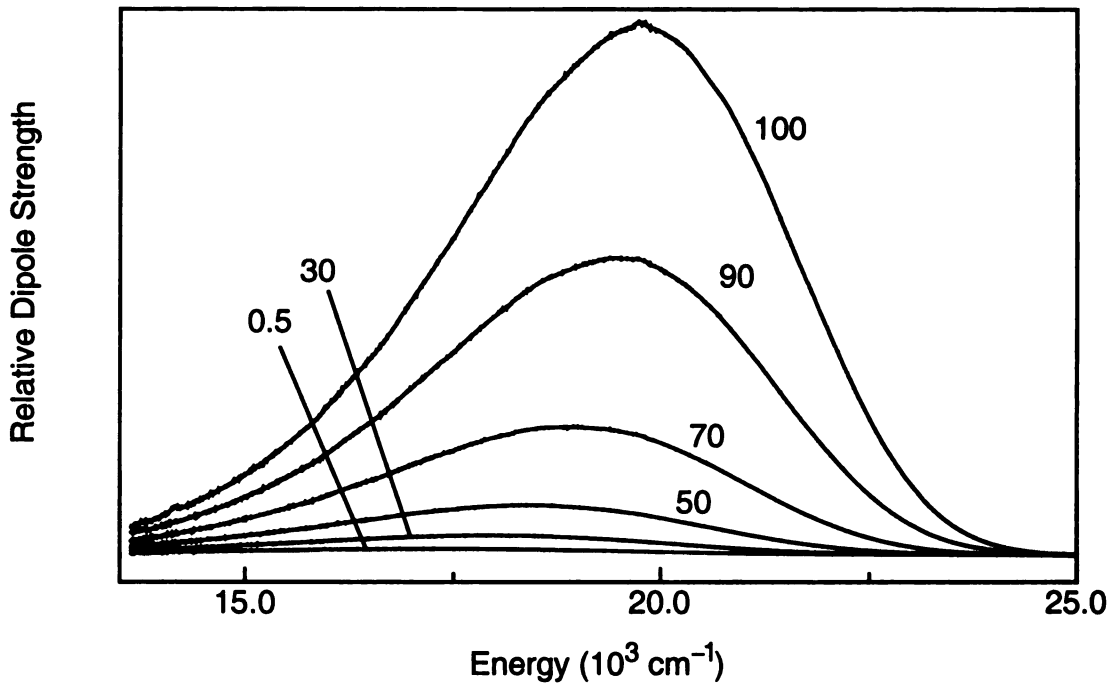

Figure 2.4. Fluorescence dipole-strength spectra from 20 μM ANSA solutions with decreasing methanol:water ratios. The percentage of methanol in the methanol/water solvent mixture is shown beside each spectrum.

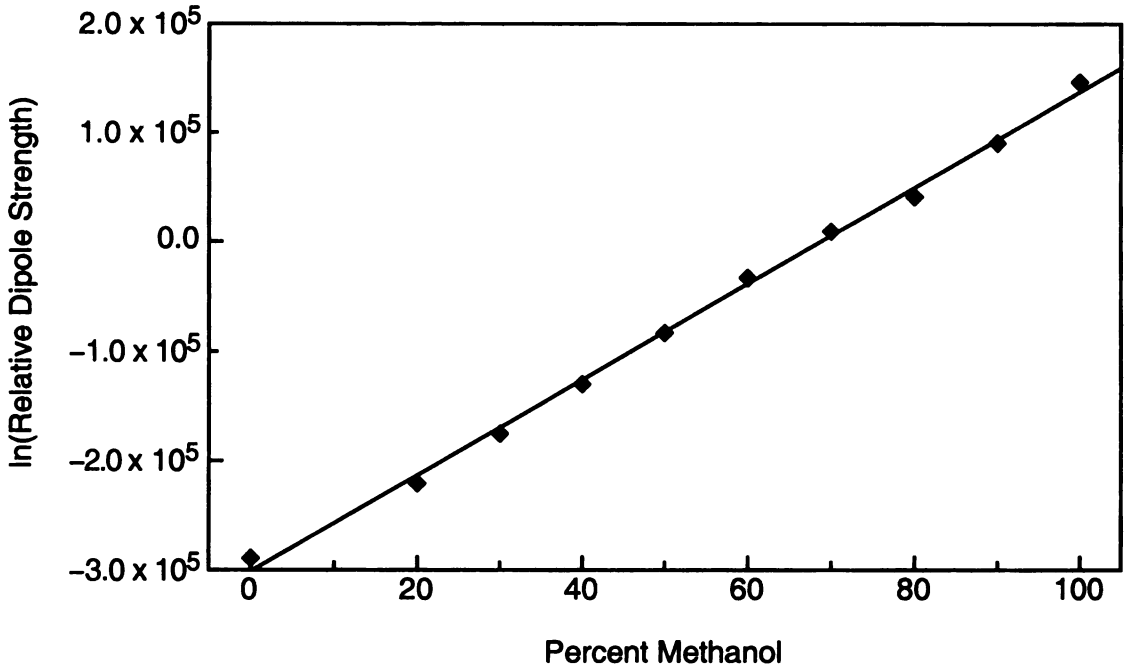

Figure 2.5. Progression of the integrated relative fluorescence dipole strength from 20 μM ANSA solutions with increasing methanol:water ratios. Each data point represents the ln(total dipole strength) of the ANSA fluorescence spectrum obtained by fitting the spectrum to a log-normal lineshape.

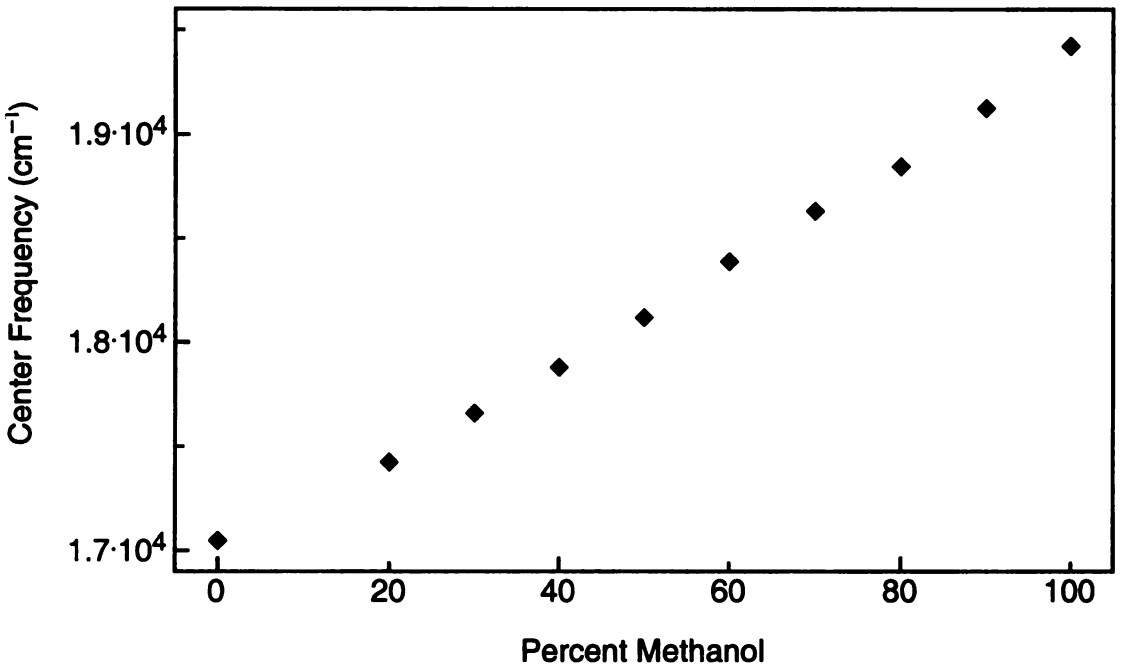

Figure 2.6. Progression of the center frequency of the ANSA fluorescence spectrum from 20 μM ANSA solutions with increasing methanol:water ratios. Each data point represents the center frequency of the ANSA fluorescence spectrum obtained by fitting the spectrum to a log-normal lineshape.

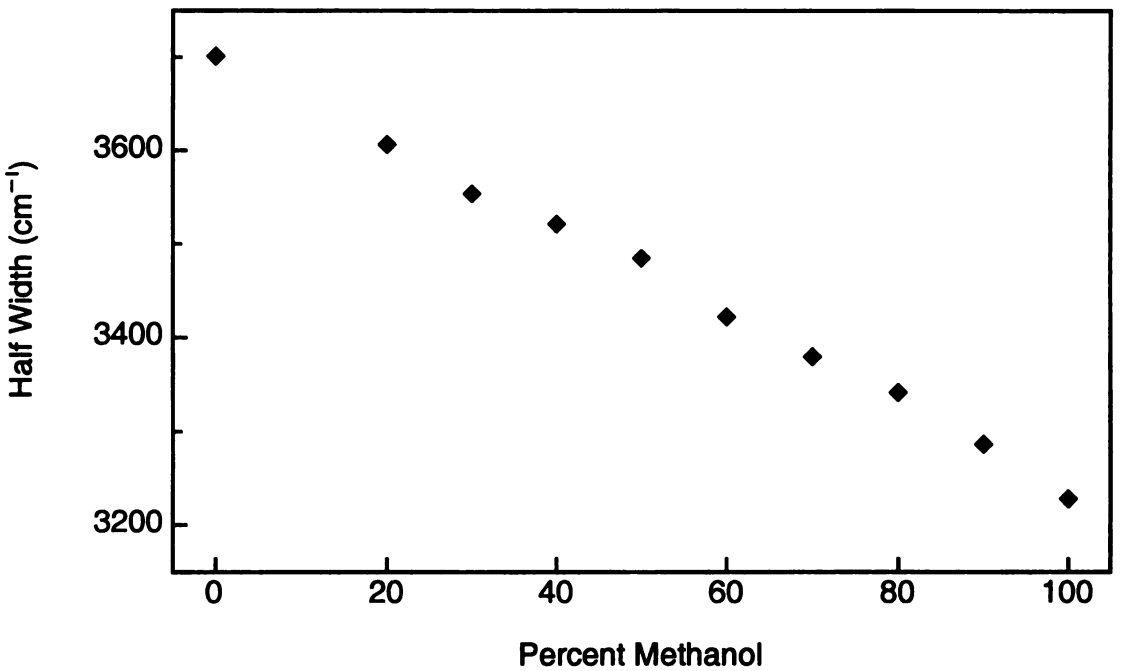

Figure 2.7. Progression of the half-width at half-maximum of the ANSA fluorescence spectrum from 20 μM ANSA solutions with increasing methanol:water ratio. Each data point represents the half-width at half-maximum of the ANSA fluorescence spectrum obtained by fitting the spectrum to a log-normal lineshape.

Figure 2.6 shows the center frequency of the ANSA fluorescence spectrum as a function of methanol concentration. The observed linear response arises from the change in polarity of the solvent.[17] With a decrease in polarity of the solvent, the ANSA fluorescence spectrum blue shifts from 17047 cm^{-1} in 99.5 percent water to 19423 cm^{-1} in 100 percent methanol. As the polarity decreases, the spectrum shifts to the blue because the $S_0 \rightarrow S_1$ transition increases the dipole moment of the chromophore.

The half-width at half-maximum of the ANSA fluorescence spectrum, as shown in Figure 2.7, decreases linearly with an increase in methanol concentration. In the solution with 100 percent methanol, the half-width at half-maximum of the ANSA fluorescence spectrum is 3220 cm^{-1}, whereas in the 0.5 percent methanol solution the half-width at half-maximum of the ANSA fluorescence spectrum is 3700 cm^{-1}. This relatively small change in the width of the spectrum probably reports the change in hydrogen-bonding structure that accompanies the solvent change.

Having recorded the change in the ANSA fluorescence spectrum as a function of methanol concentration, we can now use the change in lineshape as a measure of solvent polarity. This information can be used to monitor the flow of water molecules into the hydrophobic core of an unfolding protein.

The progression of the ANSA fluorescence spectrum from a 5:10 μM ANSA:BLA solution as a function of temperature from 4 °C to 90 °C is shown in Figure 2.8. All spectra were collected with 30-second integrations and 40 averaged accumulations. The sample was allowed to equilibrate for approximately ten minutes following each temperature change before collection of the spectrum. The ANSA fluorescence spectrum shifts to the red and decreases in area as the temperature increases.

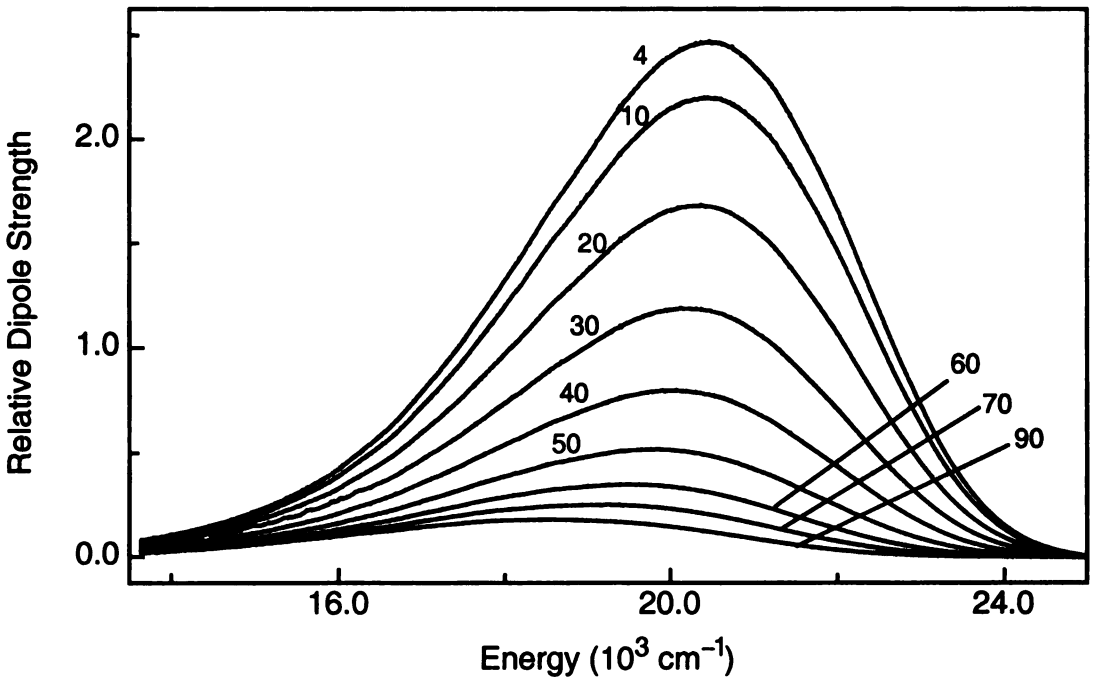

Figure 2.8. Progression of the ANSA fluorescence spectrum from a 5:10 μM ANSA:BLA solution as the temperature of the sample was increased from 4 °C to 90 °C. The temperature (°C) at which the spectrum was collected is indicated. With the increase in temperature, the ANSA fluorescence spectrum broadens and red shifts from being centered at 20180 cm^{-1} at 4 °C to 18310 cm^{-1} at 90 °C.

Figures 2.9–2.11 report the change in lineshape of the ANSA fluorescence spectrum as a function of temperature. The spectrum obtained at a given temperature was fit to a log-normal lineshape. As in the methanol solution, the skew of the lineshape was held constant at 1.14; this parameter does not change measurably as the temperature of the solution changes.

Figure 2.9 shows the progression of the area of the ANSA fluorescence spectrum with the change in solution temperature. Each data point represents an average from a set of three experiments. Error bars mark +/- one standard deviation. The area of the ANSA fluorescence spectrum is proportional to the relative total dipole strength, which is proportional to the fluorescence quantum yield. As the temperature increases from 4 °C to 90 °C, the area of the ANSA fluorescence spectrum decreases by a factor of 12.

The center frequency of the ANSA fluorescence spectrum as a function of temperature is plotted in Figure 2.10. Each data point represents an average from a set of three experiments. Error bars mark +/- one standard deviation. The center frequency of the ANSA spectrum exhibits a shift to the red a total of 1800 cm^{-1}, from 20170 cm^{-1} at 4 °C to 18370 cm^{-1} at 90 °C. This 1800 cm^{-1} shift in center frequency corresponds to a red shift of 48.6 nm.

The half-width at half-maximum of the ANSA fluorescence spectrum, as shown in Figure 2.11, increases with the change in solution temperature. From 3207 cm^{-1} at 4 °C, the half-width at half-maximum of the spectrum increases to 3383 cm^{-1} at 90 °C. The half-width of the spectrum in the BLA solution at 90 °C is comparable to that from the 70 percent methanol solution (see Figure 2.7).

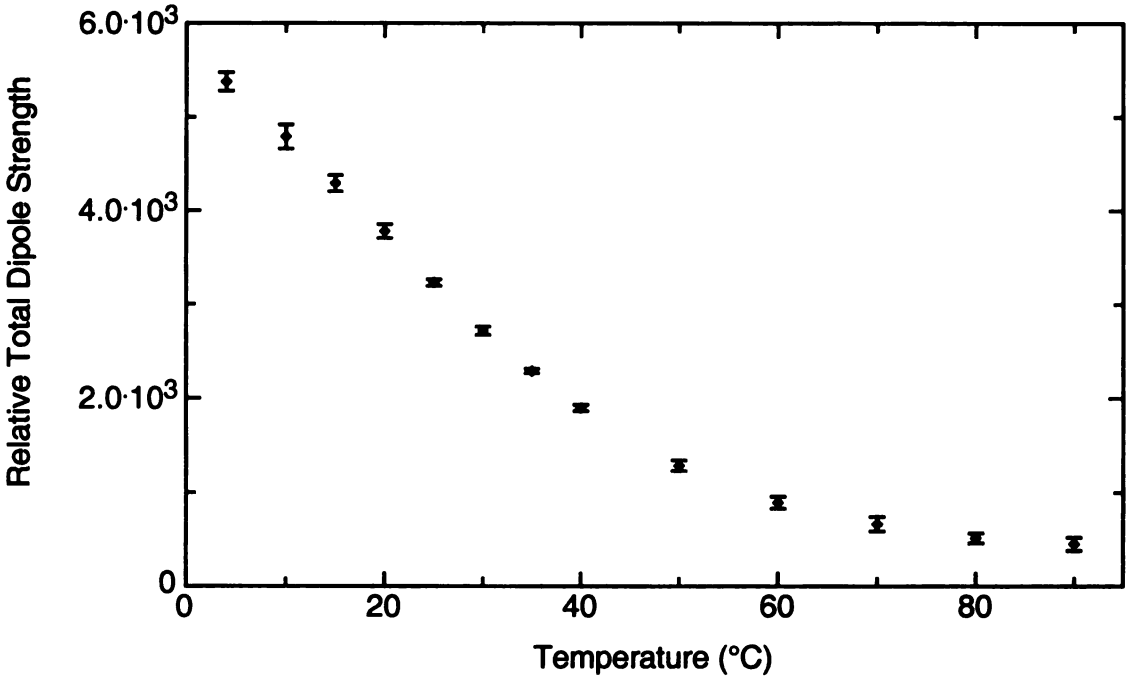

Figure 2.9. Evolution of the integrated dipole strength of the ANSA fluorescence spectrum in a 5:10 μM ANSA:BLA solution as the solution was heated from 4 °C to 90 °C. The average integrated dipole strength from a set of three experiments is plotted. Error bars mark +/- one standard deviation.

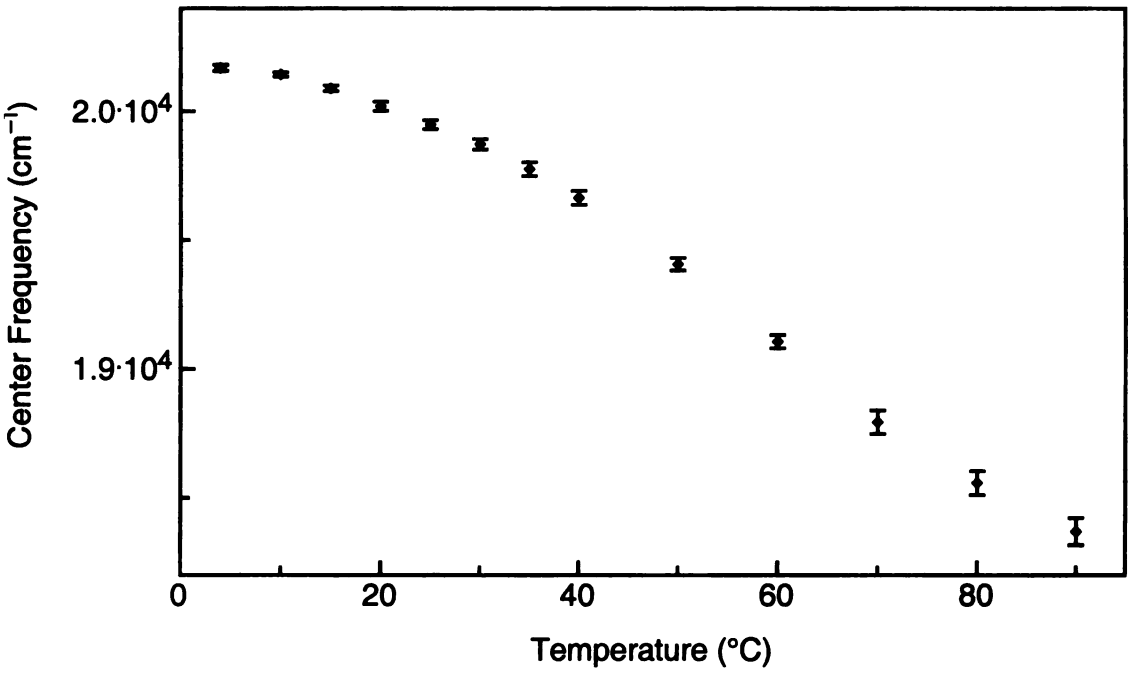

Figure 2.10. Evolution of the center frequency of the ANSA fluorescence spectrum from a 5:10 μM ANSA:BLA solution as a function of temperature from 4 °C to 90 °C. The average center frequency from a set of three experiments is shown. Error bars mark +/- one standard deviation.

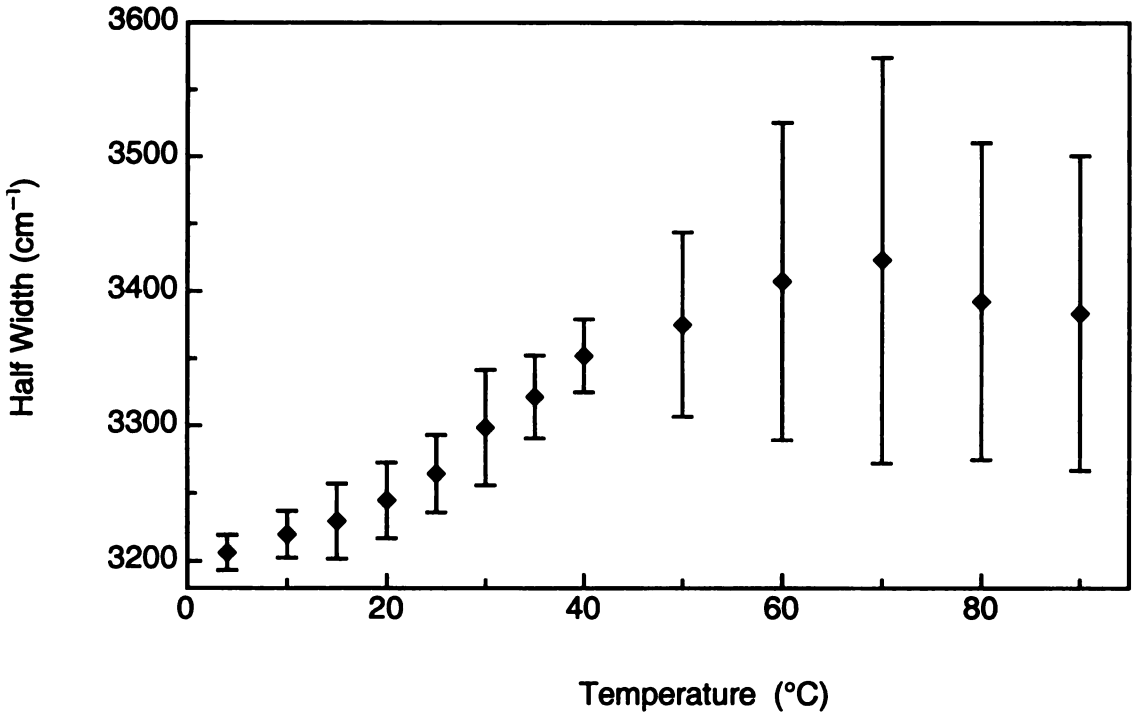

Figure 2.11. Evolution of the half-width at half-maximum of the ANSA fluorescence spectrum in a 5:10 μM ANSA:BLA solution upon heating of the solution from 4 °C to 90 °C. The average half-width at half-maximum from a set of three experiments is shown. Error bars mark +/- one standard deviation.

Discussion

The results in this chapter show that it is possible to monitor solvent motions in the unfolding of a MG through use of a solvatochromic probe. Analysis of the ANSA fluorescence spectrum from solutions with varying methanol concentrations provides a characterization of the spectral lineshape with respect to the solvent polarity. The polarity of the ANSA environment in the BLA solution can be interpreted based on this initial lineshape characterization.

As the percentage of methanol increases from 0.5 to 100 percent, the area of the ANSA fluorescence spectrum increases 78-fold, the center frequency blue shifts 2375 cm^{-1}, and the half-width at half-maximum narrows 470 cm^{-1}. These changes in lineshape are consistent with a solvatochromic dye being located in an increasingly less polar environment.[17,20]

A comparison to the results from the methanol experiments provides a rough estimate of the polarity of the ANSA environment in the BLA solution. Changes in the polarity of the probe's environment indicate a flow of solvent, in this case water, into or out of the hydrophobic core of the protein. As the temperature of the BLA solution increases from 4 °C to 90 °C, the area of the ANSA spectrum decreases by a factor of 12, the center frequency red shifts 1800 cm^{-1}, and the half-width at half-maximum broadens by 180 cm^{-1}. These parameters indicate that as the temperature increases, the average polarity of the environment surrounding the probe increases. This data is consistent with the ANSA binding to the hydrophobic core of the MG at 4 °C and then being exposed to water as the MG unfolds with the increase in temperature.

The center frequency and half-width at half-maximum of the ANSA fluorescence spectrum in the BLA solution at 4 °C both indicate that the ANSA is initially in a region that is less polar than the polarity of the 100 percent methanol sample. The center frequency of the ANSA spectrum in BLA at 50 °C is equivalent to the center frequency of the spectrum from the 100 percent methanol sample. The half-width at half-maximum of the ANSA spectrum in the 100 percent methanol sample is equal to the half-width at half-maximum of the spectrum from BLA at 15 °C. In the BLA solution at 90 °C, the center frequency of the ANSA spectrum is equal to that from a 60 percent methanol sample and the half-width at half-maximum is equal to that expected from a solution of 70 percent methanol.

Figure 2.12 compares the 5 μM ANSA dipole-strength fluorescence spectrum from four solutions. The ANSA fluorescence spectrum in methanol, 5:10 μM ANSA:BLA at 4 °C and 90 °C, and pH 2.0 water is shown in the upper panel. The bottom panel shows an expanded view of the ANSA fluorescence spectrum from the BLA solution at 90 °C and from the pH 2.0 water. The center frequency of the ANSA fluorescence spectrum is blue shifted 750 cm^{-1} in the ANSA:BLA solution at 4 °C as compared to the spectrum in the methanol sample. This suggests that at 4 °C, the ANSA in the BLA solution is located in a region that is less polar than methanol.

At 90 °C, the area of the ANSA:BLA fluorescence spectrum is four times larger than the fluorescence spectrum in the water sample. The center frequency of the ANSA:BLA spectrum at 90 °C also shifts approximately 1375 cm^{-1} to the blue of the center frequency of the ANSA spectrum in water. The parameters of these spectra obtained from fits to log-normal lineshapes are listed in Table 2.1.

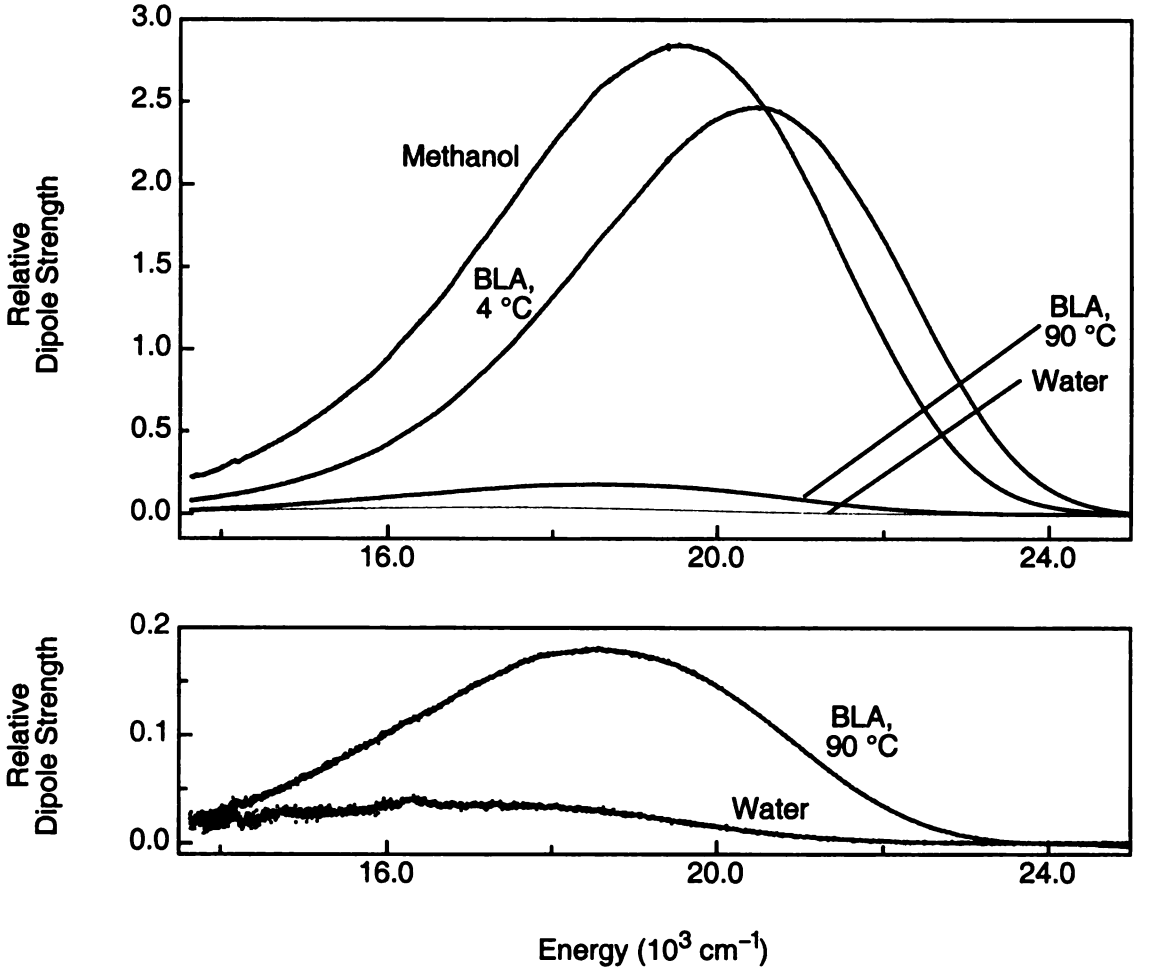

Figure 2.12. Comparison of the fluorescence dipole-strength spectrum of 5 μM ANSA in methanol, water and a 5:10 μM ANSA:BLA solution at 4 and 90 °C. The bottom panel shows an expanded view of the ANSA fluorescence spectrum from the 5:10 μM ANSA:BLA solution at 90 °C and 5 μM ANSA in pH 2.0 water.

Table 2.1. Parameters obtained by fitting the 5 μM ANSA fluorescence spectrum from methanol, 5:10 μM ANSA:BLA at 4 °C and 90 °C, and water to a log-normal lineshape. The relative area of the ANSA spectrum from methanol has been set to unity.

Sample	Relative Area	Center (cm^{-1})	Half-width at half-maximum (cm^{-1})
Methanol	1.0	19200	3310
5:10 μM ANSA:BLA, 4 °C	0.84	20181	3220
5:10 μM ANSA:BLA, 90 °C	0.067	18313	3490
Water	0.017	16936	3930

Dobson and coworkers report that the process by which *apo*-BLA, BLA in the absence of the Ca^{2+} ion, in the fully unfolded state refolds into a MG can be fit to a two-state model.[14] They studied the fluorescence anisotropy of *apo*-BLA as it refolds from the guanidinium chloride-denatured fully unfolded state to the native state (pH 7.0) and to the MG (pH 2.0) by mixing with a refolding buffer and attribute the burst-phase anisotropy in the folding to the native state to the formation of a MG. They fit the anisotropy data from the formation of the MG to a two-state model. Arai and Kuwajima also attribute the burst-phase intermediate in their stopped-flow far UV CD and fluorescent measurements to the formation of a kinetic MG during the refolding of α-lactalbumin from the unfolded state to the native state.[15] They report that the only intermediate in the refolding process is the MG and model the UV CD data of unfolding of the MG state to a two-state transition. Not only do they look at the kinetic unfolding transition, they also report the equilibrium and theoretical unfolding transition as being a two-state transition.

A two-state model suggests that as the MG-state of BLA unfolds, there is a smooth transition between only two forms, the MG state and the unfolded state. For a two-state transition, all measures of spectroscopic data should change at the same time in accordance with the change in position of the two-state equilibrium.[3] The mid-points of the center frequency and half-width at half-maximum of the unfolding transition would be expected to occur at the same temperature if the transition were really two-state in character (see Figures 2.5 and 2.6).

The data in this chapter show the mid-point temperature of the center-frequency transition is approximately 53 °C, whereas that of the half-width at half-maximum

transition is roughly 33 °C. This implies that the unfolding of the MG state to the unfolded state is highly heterogeneous. The ensemble of proteins apparently moves through a variety of forms, each with a distinct contribution to the ANSA spectrum and with a distinct temperature, as the unfolding proceeds.

Semisotnov and Dobson have reported that as the acid-denatured MG of α-lactalbumin is heated, it unfolds to a fully unfolded state.[5,21] Semisotnov also reports that the fully unfolded state does not bind ANSA.[21] The data presented here, however (see Figure 2.12 and Table 2.1), suggest there is residual structure in the BLA that provides a binding site for the ANSA even at 90 °C. Redfield also reports that ANSA in solution with the chemically-denatured, fully unfolded state of human α-lactalbumin exhibits a fluorescence spectrum that differs from the dye in free in water.[22]

If the BLA were fully unfolded to a random-coil state, the dye molecule would be surrounded by water and have spectral properties very similar to the free dye in water. Our results indicate that at the end of the thermal unfolding transition, the BLA molecule retains a folded region that binds ANSA and partially protects it from the bulk aqueous environment.

The results in this chapter show that the lineshape of the ANSA probe provides a great deal of information over that provided by the intensity alone. The center frequency of the spectrum is a rather sensitive probe to polarity. The width of the spectrum may be useful as a measure of the breadth of the structural ensemble in some cases, but here its sensitivity to the bonding structure is the main effect noted.

References

(1) Voet, D.; Voet, J. G.; Pratt, C. W. *Fundamentals of Biochemistry*; John Wiley & Sons, Inc.: New York, 1999.

(2) Ptitsyn, O. "The Molten Globule State." In *Protein Folding*; Creighton, T., Ed.; W. H. Freeman and Company: New York, 1992, p 243–300.

(3) Fersht, A. *Structure and Mechanism in Protein Science*; W. H. Freeman and Company: New York, 1999.

(4) Chrysina, E. D.; Brews, K.; Acharya, K. R. "Crystal Structures of Apo- and Holo-bovine α-Lactalbumin at 2.2–A Resolution Reveal an Effect of Calcium on Inter-lobe Interactions." *J. Biol. Chem.* **2000**, *275*, 37021–37029.

(5) Baum, J.; Dobson, C. M.; Evans, P. A.; Hanley, C. "Characterization of a Partly Folded Protein by NMR Methods: Studies on the Molten Globule State of the Guinea Pig α-Lactalbumin." *Biochemistry* **1989**, *28*, 7–13.

(6) Schulman, B. A.; Redfield, C.; Peng, Z.; Dobson, C. M.; Kim, P. S. "Different Subdomains are Most Protected from Hydrogen Exchange in the Molten Globule and Native States of Human α–Lactalbumin." *J. Mol. Biol.* **1995**, *253*, 651–657.

(7) Balbach, J.; Forge, V.; Lau, W. S.; Jones, J. A.; van Nuland, N. A. J.; Dobson, C. M. "Detection of residue contacts in a protein folding intermediate." *Proc. Natl. Acad. Sci. USA* **1997**, *94*, 7182–7185.

(8) Forge, V.; Wijesinha, R. T.; Balbach, J.; Brew, K.; Robinson, C. V.; Redfield, C.; Dobson, C. M. "Rapid Collapse and Slow Structural Reorganisation During the Refolding of Bovine α-Lactalbumin." *J. Mol. Biol.* **1999**, *288*, 673–688.

(9) Chakraborty, S.; Ittah, V.; Bai, P.; Luo, L.; Haas, E.; Peng, Z. "Structure and Dynamics of the α–Lactalbumin Molten Globule: Fluorescence Studies Using Proteins Containing a Single Tryptophan Residue." *Biochemistry* **2001**, *40*, 7228–7238.

(10) Kuwajima, K. "The molten globule state of α-lactalbumin." *FASEB J.* **1996**, *10*, 102-109.

(11) Vendruscolo, M.; Paci, E.; Karplus, M.; Dobson, C. M. "Structures and relative free energies of partially folded states of proteins." *Proc. Natl. Acad. Sci. USA* **2003**, *100*, 14817.

(12) Semisotnov, G. V.; Kihara, H.; Kotova, N. V.; Kimura, K.; Amemiya, Y.; Wakabayashi, K.; Serdyuk, I. N.; Timchenko, A. A.; Chiba, K.; Nikaido, K.; Ikura, T.; Kuwajima, K. "Protein Globularization During Folding. A Study by Synchrotron Small-angle X-ray Scattering." *J. Mol. Biol.* **1996**, *262*, 559–574.

(13) Rawitch, A. B.; Hwan, R.-Y. "Anilinonaphthalene sulfonate as a probe for the native structure of bovine alpha lactalbumin: Absence of binding to the native, monomeric protein." *Biochemical and Biophysical Research Communications* **1979**, *91*, 1383–1389.

(14) Canet, D.; Doering, K.; Dobson, C. M.; Dupont, Y. "High–Sensitivity Fluorescence Anisotropy Detection of Protein–Folding Events: Application to α–Lactalbumin." *Biophys. J.* **2001**, *80*, 1996–2003.

(15) Arai, M.; Kuwajima, K. "Rapid formation of a molten globule intermediate in refolding of α–lactalbumin." *Folding and Design* **1996**, *1*, 275–287.

(16) Vanderheeren, G.; Hanssens, I. "Thermal unfolding of bovine α-lactalbumin." *J. Biol. Chem.* **1994**, *269*, 7090–7094.

(17) Lakowicz, J. R. *Principles of Fluorescence Spectroscopy*; Second ed.; Kluwer Academic/Plenum Publishers: New York, 1999.

(18) Cantor, C. R.; Schimmel, P. R. *Biophysical Chemistry. Part II: Techniques for the Study of Biological Structure and Function*; W. H. Freeman and Company: San Francisco, 1980.

(19) Siano, D. B.; Metzler, D. E. "Band shapes of the electronic spectra of complex molecules." *J. Chem. Phys.* **1969**, *51*, 1856–1861.

(20) Turner, D. C.; Brand, L. "Quantitative Estimation of Protein Binding Site Polariy. Fluorescence of *N*–Arylaminonaphthalenesulfonates." *Biochemistry* **1968**, *7*, 3381–3390.

(21) Semisotnov, G. V.; Rodionova, N. A.; Razgulyaev, O. I.; Uversky, V. N.; Gripas, A. F.; Gilmanshin, R. I. "Study of the "Molten Globule" Intermeidate Sate in Protein Folding by a Hydrophobic Fluorescenct Probe." *Biopolymers* **1991**, *31*, 119–128.

(22) Ramboarina, S.; Redfield, C. "Structural Characterisation of the Human α–Lactalbumin Molten Globule at High Temperature." *J. Mol. Biol.* **2003**, *330*, 1177–1188.

CHAPTER 3

STUDY OF THE α-HELIX TO β-SHEET TRANSITION OF POLY-L-LYSINE USING 1-ANILINO-8-NAPHTHALENESULFONIC ACID AS A FLUORESCENT PROBE AND LIGHT SCATTERING

Introduction

In the 1960's, Davidson and Fasman showed that by heating poly-L-lysine (PLL) at pH 11 to around 50 °C, the initially α-helical form converts quantitatively to the β-sheet form in a few minutes.[1,2] These early CD measurements suggest that this conformational transition involves an equilibrium between the α-helix form and a random coil at temperatures below the temperature required for the β-sheet formation.[1,3] At temperatures above that required for the β-sheet formation, however, the rate of formation of the β-sheet is very rapid.[4] Witz and Van Duuren then studied the three forms of PLL, the α-helix form, random coil, and β-sheet form, with a hydrophobic fluorescence probe, 2-*p*-toluidinylnaphthalene-6-sulfonate (TNS), which is very similar in structure to ANSA.[5] They conclude that TNS binds preferentially to the β-form of PLL and does not bind to either the α-helix or random-coil species. Dzwolak and coworkers have recently used FTIR spectroscopy to detect a transition-state species that precedes the formation of the β-sheet form.[6] They suggest that the structure of the transition state contains neither a true α-helix nor a pure β-sheet secondary-structural compliment and that it partially exposes the hydrophobic regions to the bulk solvent.[7]

We are interested in the transition of PLL from the α-helix to the β-sheet form because of the relevance of such a transition in the formation of amyloid fibrils that are associated with diseases. The tendency to form amyloid fibrils is apparently a general

property of polypeptides and not necessarily dependent on specific amino-acid sequences or native-fold topologies.[8] Even proteins with globular structures that have primarily α-helical secondary structure have been shown to form amyloid fibrils.[9,10] In order for these amyloid fibrils to form, some of the α helices have to unfold and then refold to form β-sheet-rich structures.[9]

In this chapter, we monitor the conformational transition of PLL from the α-helical form to the β-sheet form with an extrinsic probe, ANSA. The lineshape of the ANSA fluorescence spectrum has been characterized with respect to polarity in Chapter 2 of this thesis. We chose to characterize the ANSA fluorescence spectrum in the MG of α-lactalbumin first because of its well-characterized structure.[11,12]

As PLL goes through the transition to the β-sheet form, the α-helical form must somehow first unfold to a less structured form, such as a MG. If a MG forms, it will bind ANSA in its hydrophobic region. By monitoring the ANSA fluorescence lineshape and the Rayleigh light-scattering peak during the secondary-structural transition, we can determine the relative rates of change of the spectral parameters and the rate of change of the molecular weight, respectively. Given our previous knowledge of the spectral response of ANSA in a well-characterized MG, we can determine if a MG-like state is formed during the PLL structural transition and what, if any, role this state plays in the rate of aggregation.

Within our spectral range for data collection, we can monitor both the ANSA fluorescence spectrum and the Rayleigh scattering peak simultaneously. The molecular weight of the solute in a polymer solution is related to the intensity of the Rayleigh scattering according to Equation 3.1.[13]

$$\frac{i_\theta}{I_0} = \frac{(1+\cos^2\theta)}{r^2} K C M_w \qquad (3.1)$$

In Equation 3.1, i_θ is the intensity of the Rayleigh scattering from the sample, I_0 is the intensity of the incident radiation, r is the distance from the sample to the detector, θ is the angle of the data collection from the incident beam, C is the concentration of the solute, M_w is the average molecular weight of the solute, and K is a constant for a given solution of macromolecules that depends on the refractive index and the monitoring wavelength.

Since we do not change the concentration of the solute during the course of the experiment, and since K is a constant for the solution at a specific wavelength, a change in the intensity of the Rayleigh-scattering peak can be attributed to a change in the molecular weight of the solute. This allows us to monitor the rate of aggregation of the peptide simultaneously with the measurement of the fluorescence spectrum of ANSA, which gives us information on the polarity of the environment that binds the probe.

Sample Preparation

ANSA (1-anilino–8-naphthalenesulfonic acid ammonium salt) and PLL (poly-L-lysine; molecular weight 30,000 – 70,000) were obtained from Sigma and used as received. Samples of 7:14 μM ANSA:PLL were dissolved in water to obtain an absorbance less than 0.05 at 350 nm with a 1-cm path length. The aqueous PLL samples were brought to pH 11.0 with NaOH. Prior to collection of fluorescence spectra, samples were passed through 0.22 μm filters (Millipore, Millex-GV). All fluorescence spectra were collected on the spectrofluorimeter described in Chapter 2. The conversion of the α-helical form to the β-sheet form was induced by increasing the temperature of the

solution from 23 °C to 55 °C using the temperature-controlled sample holder. These sample conditions were chosen based on previous work by Davidson and Fasman.[1]

Experimental

For each experiment, spectra were collected at pre-set time intervals over a minimum of two hours. Before the temperature change, the fluorescence spectra were collected by exposing the CCD for 10 accumulations of a 20-s integration time every 240 s. After the temperature change, thirty spectra were collected with 10 accumulations of a 10-s integration at 120 s intervals for the first 3600 s. Once the rate of change in the ANSA fluorescence spectrum began to decrease, the number of accumulations averaged for each spectrum was increased to 20 and the time interval between collections was increased to 900 s. Each spectrum was normalized by the exposure time of the CCD to compensate for the different exposure times over the course of the experiment.

Results

The temperature profile for a water-filled cuvette in the same experimental setup as described above is shown in Figure 3.1. The temperature on the controller was changed from 23 °C to 55 °C at the plotted zero of time. Within 330 s of changing the temperature on the controller, the solution had reached 50 °C. The temperature of the solution equilibrated to 55 °C after 540 s. Stirring was used to prevent the formation of temperature gradients within the sample.

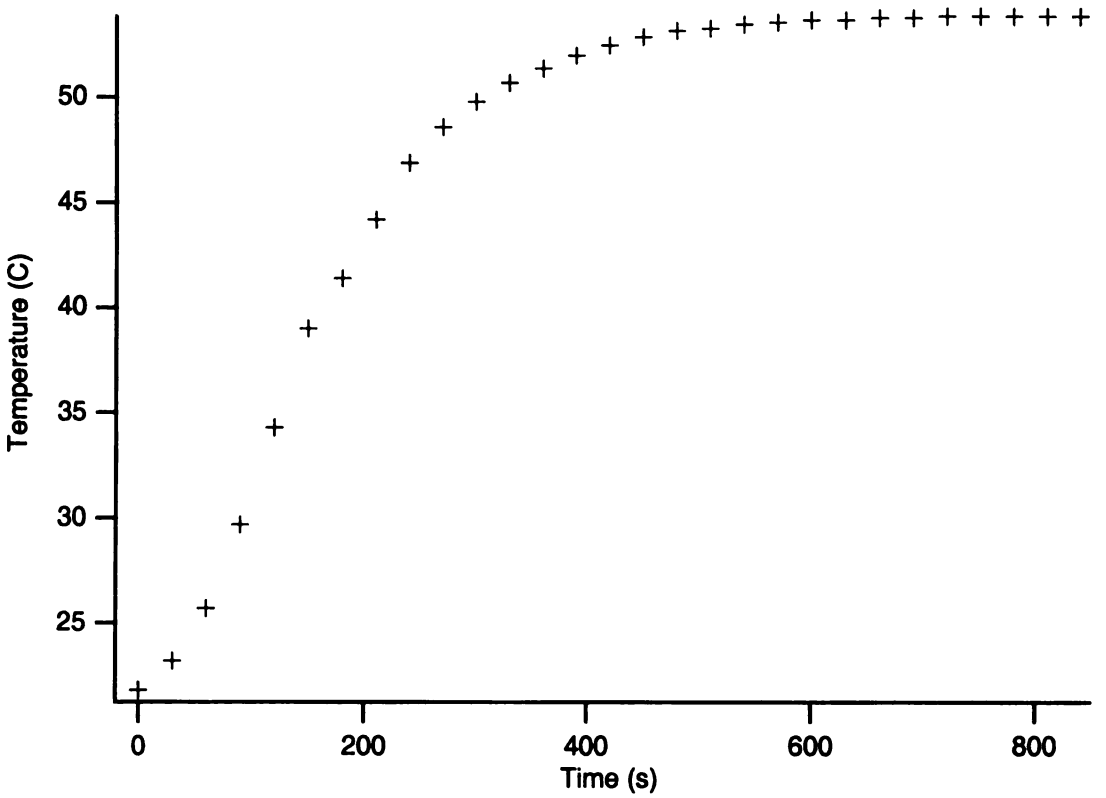

Figure 3.1. Time evolution of the temperature of the sample solution as measured by a thermocouple immersed in a blank sample of water of the same volume as used in the fluorescence experiments. The temperature controller of the sample holder was changed from 23 °C to 55 °C at the plotted zero of time. The half-time for the transition is 140 s.

After establishing the temperature profile associated with our experimental setup and conditions, we collected a series of time-resolved fluorescence spectra from solutions of 7:14 μM ANSA:PLL . Figure 3.2 shows the fluorescence spectrum collected from a 7:14 μM ANSA:PLL solution at 0 s, 580 s, and 11180 s, respectively, after the sample temperature was changed from 23 °C to 55 °C. In each spectrum, the ANSA fluorescence spectrum and scattered-light peak have been superimposed with a fit to a log-normal[14] and a Lorentzian lineshape, respectively. In the spectrum at 23 °C, prior to the change in temperature, the scattered-light peak from the 380-nm excitation source is relatively small and centered around 26600 cm^{-1}. The ANSA fluorescence spectrum, centered around 19000 cm^{-1}, is broad and relatively weak. Following the change in temperature, the relative dipole strength of the scattered-light peak increases and the ANSA fluorescence spectrum increases in dipole strength and shifts to the blue.

Expanded views of the scattered-light peak and the ANSA fluorescence spectrum, are shown in Figures 3.3 and 3.4, respectively. Figure 3.3 shows the relative dipole strength of the scattered-light peak continues to increase with time following the change in temperature without a change in lineshape. The ANSA fluorescence spectrum in Figure 3.4 reports an increase in intensity and a blue shift after the temperature change. Unlike the scattered-light peak, the ANSA fluorescence spectrum does not continue to change dramatically after 580 s. As will be shown later, the integrated dipole strength of the ANSA fluorescence spectrum levels off after the fast, initial change with the increase in temperature.

The time evolution of the average area of the scattered-light peak from a set of six experiments is plotted in Figure 3.5. Error bars mark +/- one standard deviation. The

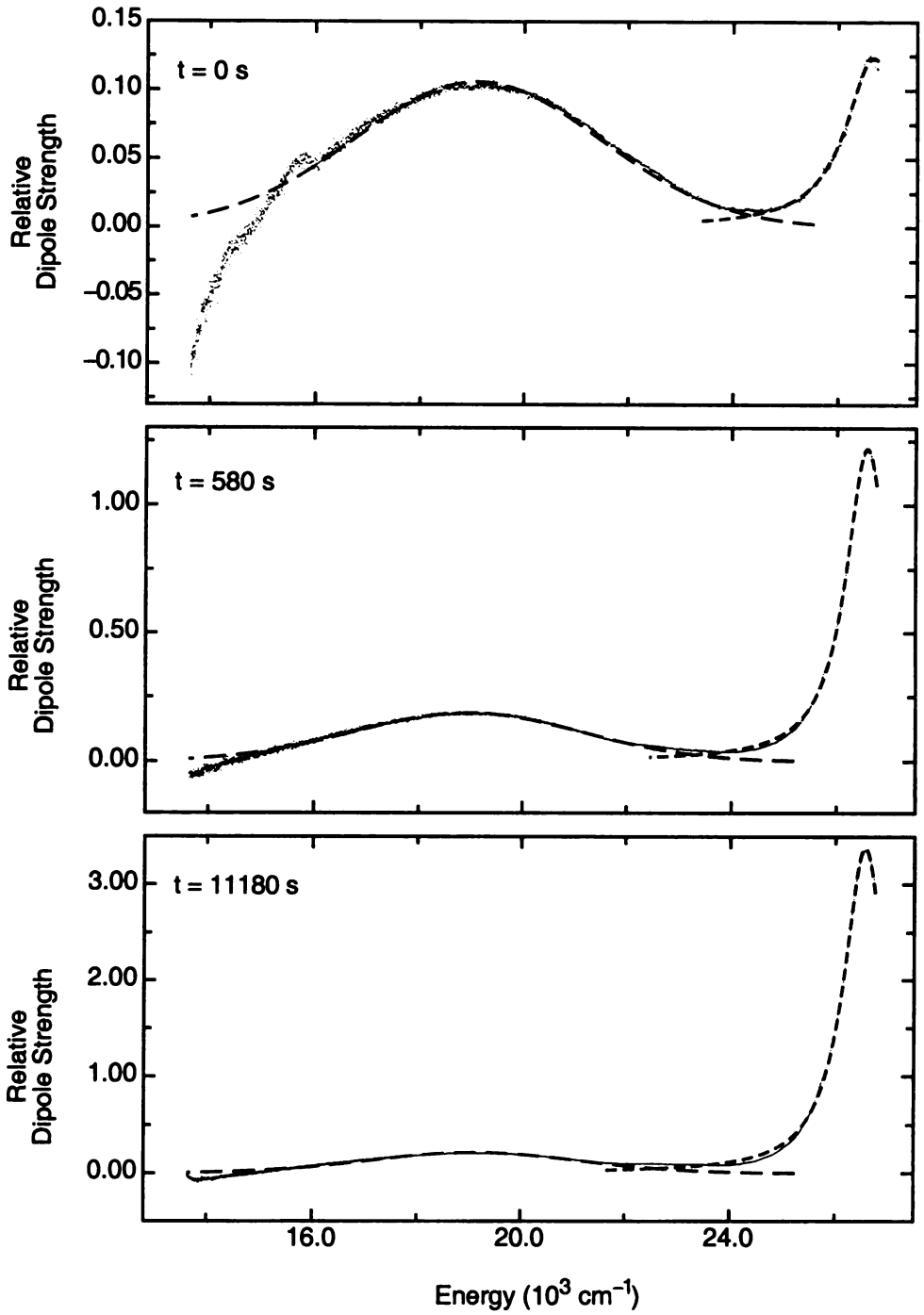

Figure 3.2. Fluorescence dipole-strength (F/ν^3) spectra from a 7:14 μM ANSA:PLL solution as a function of time following a change in temperature, from 23 °C to 55 °C. The scattered-light peak, centered at 26600 cm^{-1}, is superimposed with a fit to a Lorentzian lineshape (short dashes). The ANSA fluorescence spectrum, centered at 19000 cm^{-1}, is superimposed with a fit to a log-normal lineshape (long dashes). The indicated time is that following the sample temperature change. Note that the ordinate is autoscaled for each panel.

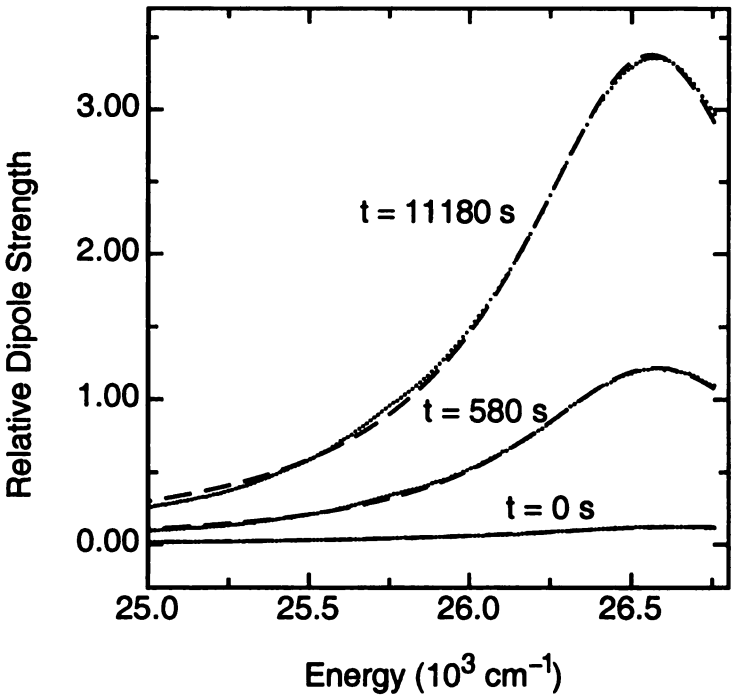

Figure 3.3. Expanded view of the time evolution of the 380 nm scattered-light peak detected in the 7:14 μM ANSA:PLL solution. The indicated time is that following the sample temperature change from 23 °C to 55 °C. The dashed lines represent the fit to a Lorentzian lineshape.

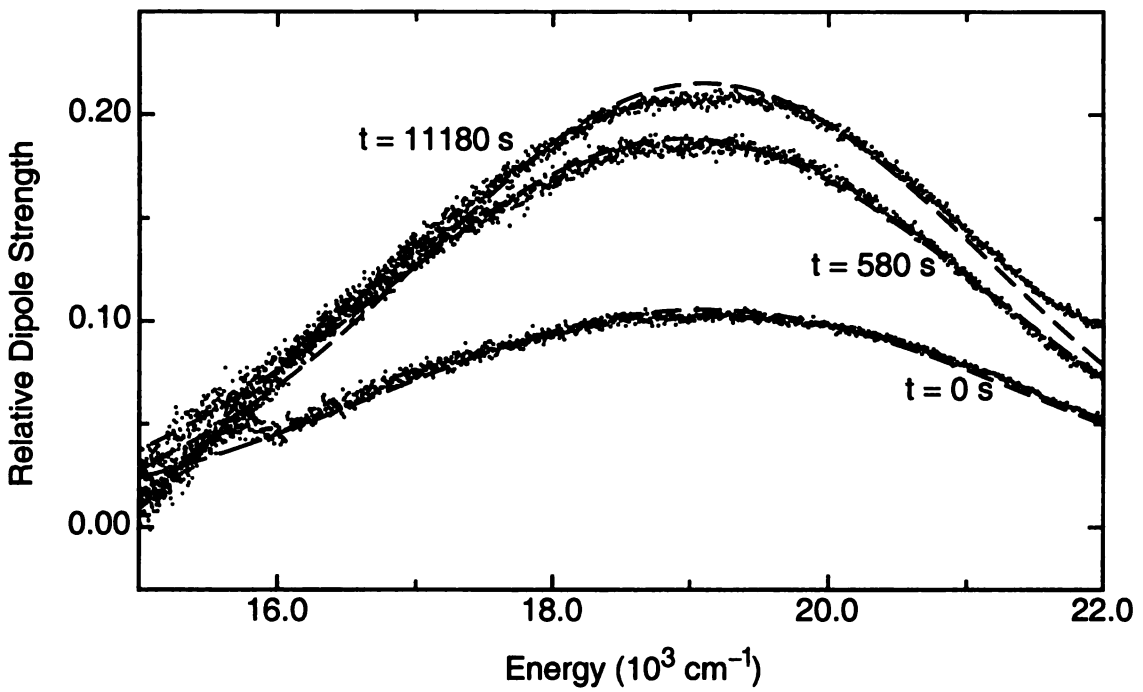

Figure 3.4. Expanded view of the time evolution of the ANSA fluorescence spectrum detected in the 7:14 μM ANSA:PLL solution. The indicated time is that following the sample temperature change from 23 °C to 55 °C. The dashed lines represent the fit to a log-normal lineshape.[14]

scattered-light peak in each spectrum was fit to a Lorentzian lineshape. From the fit to the Lorentzian lineshape, the area of the scattered-light peak was determined. The area of the scattered light peak at the zero of time was subtracted from the plotted areas. In Figures 3.5-3.8, the zero of time represents the time at which the temperature on the controller was changed from 23 °C to 55 °C. Note that the area of the scattered–light peak does not change immediately with the change in temperature. There is a 340 s delay after the temperature change before the area of the scattered–light peak changes significantly. The time constant associated with the initial exponential rise is approximately 570 s. The intensity of the scattered-light peak increases by a factor of 27, indicating the average molecular weight of the PLL increases from the initial 52 kDa to approximately 1400 kDa.

The fit of the ANSA fluorescence spectrum to a log–normal lineshape gives the total dipole strength (area), center frequency, and half–width at half–maximum of the ANSA fluorescence spectrum. The time evolution of these parameters are plotted in Figures 3.6–3.8. Each point on the time evolution plot represents the average value from a set of six experiments. Error bars mark +/- one standard deviation.

The time evolution of the total integrated dipole strength of the ANSA fluorescence spectrum in a 7:14 μM ANSA:PLL solution is shown in Figure 3.6. In response to the increase in temperature to 55 °C, the area of the ANSA fluorescence spectrum increases. The integrated area is proportional to the total dipole strength, which is proportional to the relative quantum yield.[15] The increase in area of the ANSA fluorescence spectrum is indicative of the ANSA probe being in an environment that is less polar. There appear to be at least two components in the time evolution of the area of the ANSA fluorescence

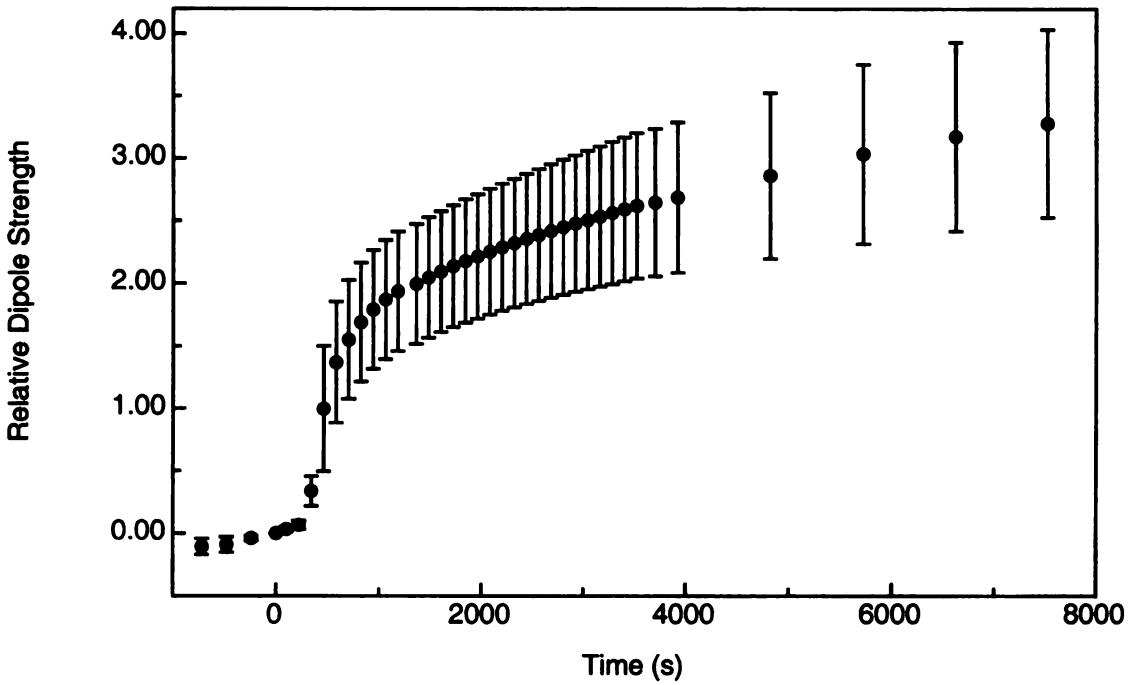

Figure 3.5. Time evolution of the area (integrated dipole strength) of the scattered-light peak observed in a 7:14 μM ANSA:PLL solution. The average area from a set of six experiments is shown. Error bars mark +/- one standard deviation. The area of the scattered light peak at the plotted zero of time (the time at which the temperature change from 23 °C to 55 °C occurred) was subtracted from the plotted areas.

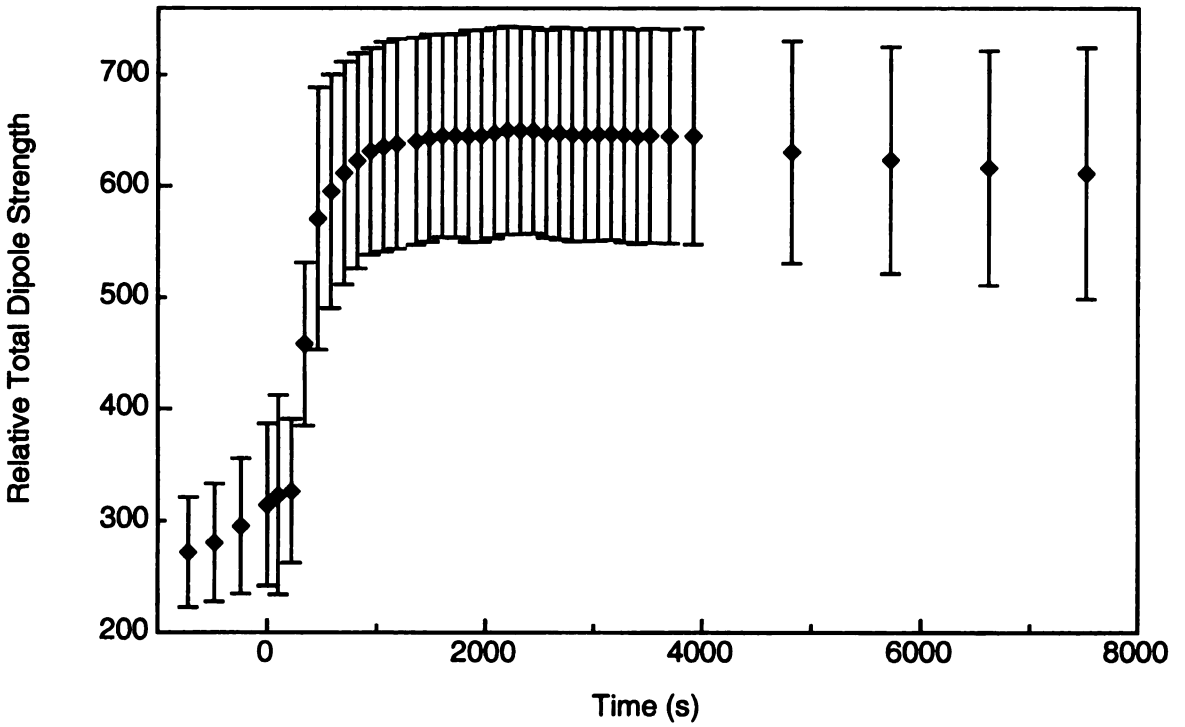

Figure 3.6. Time evolution of the integrated dipole strength of the ANSA fluorescence spectrum in a 7:14 μM ANSA:PLL solution. The average integrated dipole strength from a set of six experiments is plotted. Error bars mark +/- one standard deviation. The sample temperature was changed from 23 °C to 55 °C at the plotted zero of time.

spectrum. The initial, rapid component shows an exponential rise that is completed after approximately 1500 s. A second, slower component accompanies a decrease in the area of the ANSA fluorescence spectrum.

The time evolution of the average center frequency and the half-width at half-maximum of the ANSA fluorescence spectrum in the sample described above are shown in Figures 3.7 and 3.8, respectively. The responses of the center frequency and the half-width at half-maximum of the ANSA fluorescence spectrum to the temperature change are consistent with the ANSA probe being in a less polar environment after the increase in temperature. As shown in Figure 3.7, the center frequency of the ANSA fluorescence spectrum to shifts to the blue by 1033 cm^{-1} (32 nm) within 500 s of the temperature change. Following the initial rise, the average center frequency of the ANSA fluorescence spectrum continues a slight shift to the blue over the length of the experiment.

Figure 3.8 shows that the time evolution of the half-width at half-maximum of the ANSA fluorescence spectrum shows a rapid narrowing that is completed approximately 1000 s after the temperature change. Following the initial component, the lineshape continues a slow narrowing as time progresses. The presence of two phases in all of the parameters associated with the ANSA fluorescence spectrum suggests that there is an initial dramatic change in the structure of the PLL following the change in temperature and then a slower, more subtle change in structure occurs as the molecular weight of the PLL increases.

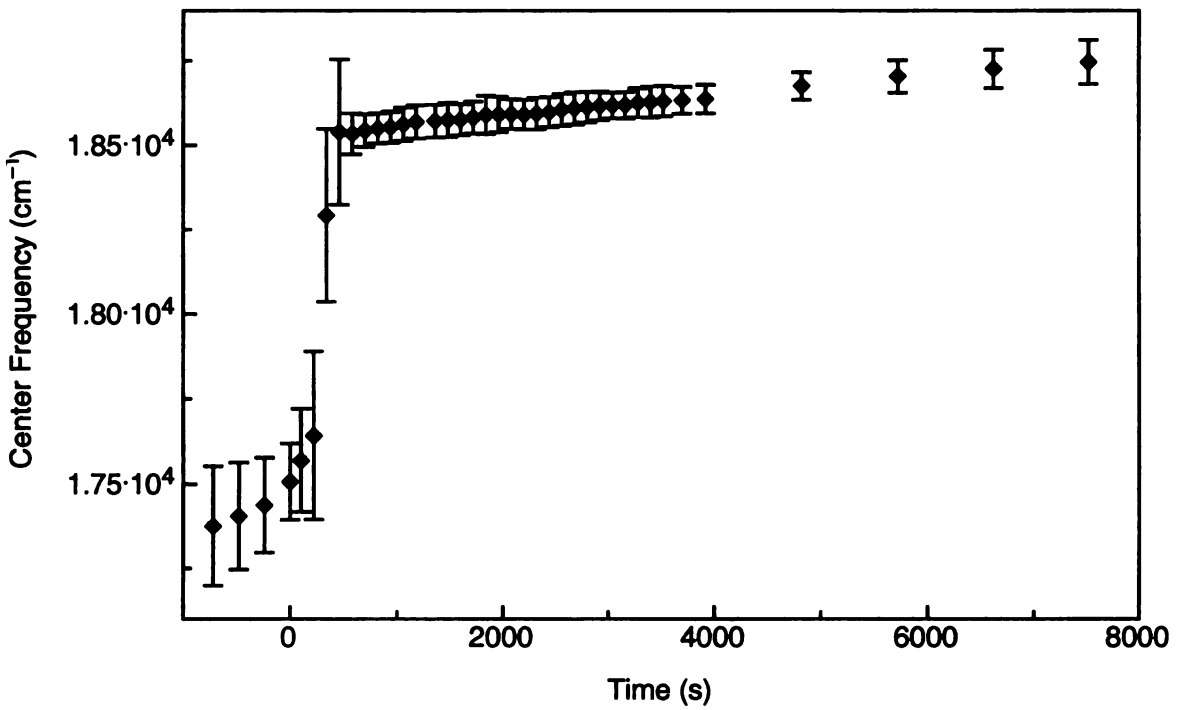

Figure 3.7. Time evolution of the average center frequency of the ANSA fluorescence spectrum observed in a 7:14 μM ANSA:PLL solution. The average center frequency from a set of six experiments is shown with error bars marking +/- one standard deviation. The sample temperature was changed from 23 °C to 55 °C at the plotted zero of time.

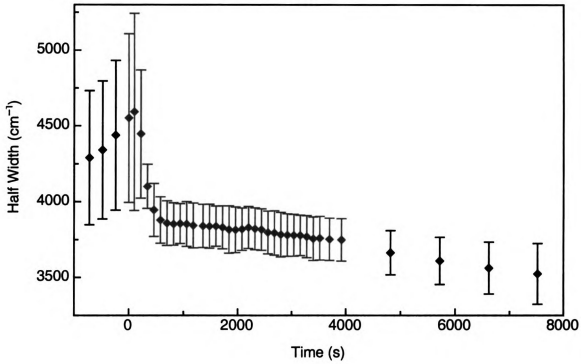

Figure 3.8. Time evolution of the half-width at half-maximum of the ANSA fluorescence spectrum in a 7:14 μM ANSA:PLL solution. The average half-width at half-maximum from a set of six experiments is shown. Error bars mark +/- one standard deviation. The sample temperature was changed from 23 °C to 55 °C at the plotted zero of time.

Discussion

With the change in temperature from 23 °C to 55 °C, the relative dipole strength of the scattered-light peak from the ANSA:PLL solution shows a 340-s delay in response, a rapid increase that is completed within the first 2000 s, and then a slower, continual increase with time. The concentration of the sample is constant throughout the experiment, so the increase in the Rayleigh scattering can be attributed to the increase in average molecular weight of the solute (see Equation 3.1).

The area, center frequency, and half-width at half-maximum of the ANSA fluorescence spectrum show a delay of approximately 220 s that precedes the initial rapid response to the increase in temperature. The responses of these parameters appear to be associated with at least two time constants, a fast initial response and a second, much slower response. The area of the fluorescence spectrum doubles within 2200 s after the increase in temperature and then shows a slight decrease with time. Over the time of the data collection, the center frequency of the spectrum shifts 1240 cm^{-1} to the blue and the half-width at half-maximum decreases by 925 cm^{-1} after the initial 220 s delay in response.

The experimental setup used in this thesis has an inherent time lag associated with the change in sample temperature. The 220-s delay in the response of the ANSA fluorescence spectrum most likely arises from the sample being at a temperature below that required for the β-sheet formation due to this time lag. As shown in Figure 3.1, 220 s after the temperature change on the controller, the temperature of the solution is approximately 45 °C, which should be a high enough temperature to allow formation of β-sheet under our conditions.[1]

Figure 3.9 shows the relative rates of the spectral responses from the ANSA:PLL solution shown in Figures 3.5–3.8. The relative rates of change in order from fastest to slowest are as follows: center frequency, half-width at half-maximum, area, and light scattering. Snell and Fasman report a rate of β-sheet formation at 55 °C that has an exponential time constant of approximately 50 s, but the differences in our experimental setups do not allow direct comparison of these data with ours.[4] It is likely that once our system has reached 55 °C, the formation of the β-sheet occurs on the same time scale.

The center frequency of the ANSA spectrum is the parameter that is most sensitive to the polarity of the environment. Its relatively fast rate of change suggests that a species with hydrophobic binding sites for the probe is formed rapidly upon heating. This species, which binds ANSA, can be considered MG-like.

Dzwolak and coworkers have suggested a transition-state species that is less structurally defined than either a pure α-helix or a pure β-sheet and has hydrophobic regions exposed . They suggest that the formation of a "loose" helix would allow exposure of hydrophobic binding sites for ANSA.[7] Our data is in agreement with the formation of a species that binds ANSA prior to the formation of aggregates. It is difficult, however, to say whether we can differentiate between this MG-like state with "loose" secondary structure and the pure β-sheet form of PLL prior to aggregation.

Using the relative rates of change presented in Figure 3.9, we propose the following model for the sequence of events in the α–β transition:

$$\alpha \rightarrow \mathrm{MG} \rightarrow \left(\mathrm{MG}_n \rightarrow \beta_{\mathrm{aggregate}}\right)$$

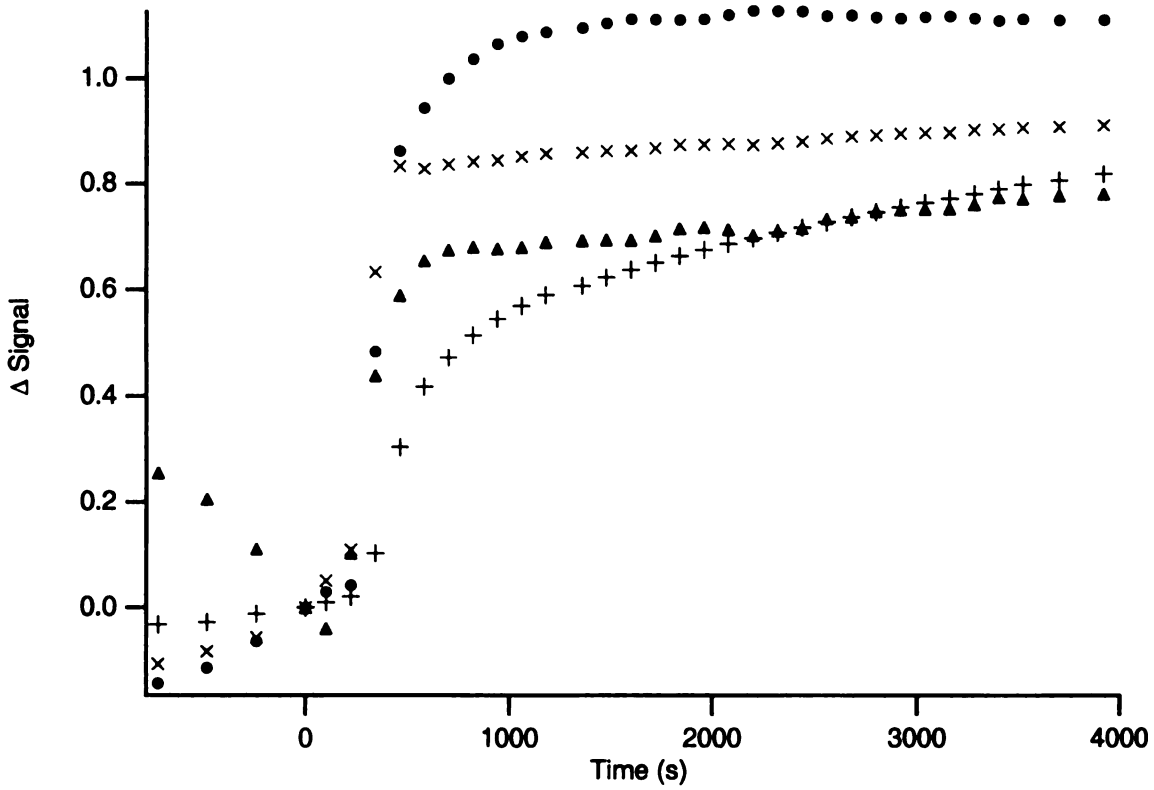

Figure 3.9. Comparison of the time evolution of the ANSA fluorescence spectrum (area (•), center frequency (×), half-width at half-maximum (▲)) and the scattered-light peak (+) from the 7:14 μM ANSA:PLL solution following a 23 °C to 55 °C temperature change. The signals have been normalized to zero at t_0 and to unity at t = 7250 s. The ANSA half-width at half-maximum response has been inverted.

Parentheses are placed around the MG_n to $\beta_{aggregate}$ transition because we are not able to differentiate the time ordering of the formation of the aggregates from the formation of the β-sheet from our results. In the following, we discuss how the proposed mechanism is suggested by the experimental observations.

A comparison of the change in center frequency of the ANSA upon binding to the PLL with the change in the center frequency of the MG state of BLA supports the idea of a MG-like intermediate in PLL. The change in center frequency of ANSA during the thermal unfolding of the MG of BLA is 1800 cm^{-1} (48 nm, see Chapter 2) and the change in center frequency during the α–β transition in PLL is 1371 cm^{-1} (42 nm). The absolute values of the center frequencies, however, suggest that the environment of the ANSA in the PLL is more polar than the MG of BLA. In the PLL solution, the ANSA goes from being essentially free in water to an environment that is partially sheltered from the water. There is only an increase by a factor of two in the area of the ANSA fluorescence spectrum in PLL, whereas there is more than a ten-fold increase in the area of the ANSA fluorescence spectrum in the MG BLA. The relatively small increase in area in the PLL solution is likely to involve the partially-exposed nature of the binding site for ANSA in PLL. The decrease in the area over long time accompanies the formation of larger and larger aggregates. As these aggregates form, the ANSA-binding site is gradually increasingly exposed to solvent. This indicates an evolution of the initial aggregate to a different structural form.

Figure 3.8 shows that as the temperature is increased, the width of the ANSA spectrum decreases. A decrease in the width of the ANSA spectrum indicates that the range of structures in the ensemble is decreasing. As time progresses, the ANSA

spectrum continues to narrow as the aggregation (see Figure 3.5) of PLL increases. This suggests that a more ordered form accumulates as the aggregation continues.

The rate of change of the scattered-light peak is the slowest of the four parameters analyzed. This suggests that before aggregation can occur, the β-rich state of PLL must form. Experiments similar to the one reported here only with different concentrations of PLL suggest that the rates of change do not change significantly with a change in concentration of peptide (data not shown). This suggests that the initial formation of the β-sheet-rich PLL is intramolecular.

All of these changes in spectral parameters are consistent with the mechanism proposed above. In the transition from α-helix to β-sheet, the rate of formation of the β-sheet is dependent on the initial formation of the MG-like state. Note that formation of aggregates following a secondary structural transition of a protein is reminiscent of the prion and prion-related diseases. Prions are proteins that undergo conformational changes that result in accumulation of aggregate forms that are cytotoxic.[16] It may be possible that the conformational transition of PLL could be furthered considered as a model system for understanding the mechanism by which prions aggregate.

References

(1) Davidson, B.; Fasman, G. D. "The Conformational Transitions of Uncharged Poly-L-lysine. α Helix-Random Coil-β Structure." *Biochemistry* **1967**, *6*, 1616–1629.

(2) Davidson, B.; Fasman, G. D. "The Single-Stranded Polyadenylic Acid-Poly-L-lysine Complex. A Conformational Study and Characterization." *Biochemistry* **1969**, *8*, 4116–4126.

(3) Wooley, S.-Y. C.; Holzwarth, G. "Intramolecular β-Pleated-Sheet Formation by Poly-L-lysine in Solution." *Biochemistry* **1970**, *9*, 3604–3608.

(4) Snell, C. R.; Fasman, G. D. "Kinetics and Thermodynamics of the α Helix-β Transconformation of Poly(L-lysine) and L-Leucine Copolymers. A Compensation Phenomenon." *Biochemistry* **1973**, *12*, 1017–1025.

(5) Witz, G.; Van Duuren, B. L. "Hydrophobic Fluorescence Probe Studes with Poly-L-lysine." *J. Phys. Chem.* **1973**, *77*, 648–651.

(6) Dzwolak, W.; Muraki, T.; Kato, M.; Taniguchi, Y. "Chain-length dependence of alpha-helix to beta-sheet transition in polylysine: Model of protein aggregation studied by temperature-tuned FTIR spectroscopy." *Biopolymers* **2004**, *73*, 463–469.

(7) Dzwolak, W.; Smirnovas, V. "A conformational α-helix to β-sheet transition accompanies racemic self-assembly of polylysine: an FT-IR spectroscopic study." *Biophys. Chem.* **2005**, *115*, 49–54.

(8) Chiti, F.; Webster, P.; Taddei, N.; Clark, A.; Stefani, M.; Ramponi, G.; Dobson, C. M. "Designing conditions for in vitro formation of amyloid protofilaments and fibrils." *Proc. Natl. Acad. Sci. USA* **1999**, *96*, 3590–3594.

(9) Pertinhez, T. A.; Bouchard, M. L.; Tomlinson, E. J.; Wain, R.; Ferguson, S. J.; Dobson, C. M.; Smith, L. J. "Amyloid fibril formation by a helical cytochrome." *Febs Lett.* **2001**, *495*, 184–186.

(10) Fandrich, M.; Forge, V.; Buder, K.; Kittler, M.; Dobson, C. M.; Diekmann, S. "Myoglobin forms amyloid fibrils by association of unfolded polypeptide segments." *Proc. Natl. Acad. Sci. USA* **2003**, *100*, 15463–15468.

(11) Baum, J.; Dobson, C. M.; Evans, P. A.; Hanley, C. "Characterization of a Partly Folded Protein by NMR Methods: Studies on the Molten Globule State of the Guinea Pig α-Lactalbumin." *Biochemistry* **1989**, *28*, 7–13.

(12) Schulman, B. A.; Redfield, C.; Peng, Z.; Dobson, C. M.; Kim, P. S. "Different Subdomains are Most Protected from Hydrogen Exchange in the Molten Globule and Native States of Human α–Lactalbumin." *J. Mol. Biol.* **1995**, *253*, 651–657.

(13) van Holde, K. E.; Johnson, W. C.; Ho, P. S. *Principles of Physical Biochemistry*; Second ed.; Pearson Education, Inc: Upper Saddle River, NJ, 2006.

(14) Siano, D. B.; Metzler, D. E. "Band shapes of the electronic spectra of complex molecules." *Journal of Chemical Physics* **1969**, *51*, 1856–1861.

(15) Cantor, C. R.; Schimmel, P. R. *Biophysical Chemistry. Part II: Techniques for the Study of Biological Structure and Function*; W. H. Freeman and Company: San Francisco, 1980.

(16) Prusiner, S. B. "Prions." *Proc. Natl. Acad. Sci. USA* **1998**, *95*, 13363–13383.